IVYSPRING INTERNATIONAL PUBLISHER

Theranostics

2023; 13(9): 3021-3040. doi: 10.7150/thno.81826

Research Paper

Decreased miR-451a in cerebrospinal fluid, a marker for both cognitive impairment and depressive symptoms in Alzheimer's disease

Hu Feng[1,2], Panpan Hu[1,3], Yan Chen[1,2], Huaiqing Sun[1,4], Jiachen Cai[1,2], Xiaoxin He[1,2], Qiuchen Cao[1], Mengmei Yin[1,4], Yanli Zhang[1,2], Qian Li[1,2], Junying Gao[1,2], Charles Marshall[5], Chengyu Sheng[1,2], Jingping Shi[2,6]✉, Ming Xiao[1,2]✉

1. Jiangsu Key Laboratory of Neurodegeneration, Nanjing Medical University, Nanjing, 211166, China.
2. Brain Institute, Nanjing Brain Hospital, Nanjing Medical University, Nanjing, 210029, China.
3. Department of Anesthetic Pharmacology, Faculty of Anesthesiology, Naval Medical University, Shanghai, 200082, China.
4. Department of Neurology, the First Affiliated Hospital of Nanjing Medical University, Nanjing, 210029, China.
5. Alice Lloyd College, Pippa Passes, KY, USA.
6. Department of Neurology, the Affiliated Nanjing Brain Hospital of Nanjing Medical University, Nanjing, 210029, China.

✉ Corresponding authors: Jingping Shi, jingping_s@126.com; Ming Xiao, mingx@njmu.edu.cn.

Received: 2022.12.14; Accepted: 2023.04.06; Published: 2023.05.15

Abstract

Background: Alzheimer's disease (AD) patients are often accompanied by depressive symptoms, but its underlying mechanism remains unclear. The present study aimed to explore the potential role of microRNAs in the comorbidity of AD and depression.

Methods: The miRNAs associated with AD and depression were screened from databases and literature and then confirmed in the cerebrospinal fluid (CSF) of AD patients and different ages of transgenic APP/PS1 mice. AAV9-miR-451a-GFP was injected into the medial prefrontal cortex (mPFC) of APP/PS1 mice at seven months, and four weeks later, a series of behavioral and pathological analyses were performed.

Results: AD patients had low CSF levels of miR-451a, which was positively correlated with the cognitive assessment score, but negatively with their depression scale. In the mPFC of APP/PS1 transgenic mice, the miR-451a levels also decreased significantly in the neurons and microglia. Specific virus vector-induced overexpression of miR-451a in the mPFC of APP/PS1 mice ameliorated AD-related behavior deficits and pathologies, including long-term memory defects, depression-like phenotype, β-amyloid load, and neuroinflammation. Mechanistically, miR-451a decreased the expression of neuronal β-secretase 1 of neurons through inhibiting Toll-like receptor 4/Inhibitor of kappa B Kinase β/ Nuclear factor kappa-B signaling pathway and microglial activation by inhibiting activation of NOD-like receptor protein 3, respectively.

Conclusion: This finding highlighted miR-451a as a potential target for diagnosing and treating AD, especially for those with coexisting symptoms of depression.

Keywords: Alzheimer's disease, miR-451a, BACE1, depression, medial prefrontal cortex

Introduction

Alzheimer's disease (AD) is the most prevalent neurodegenerative disease in the elderly, with a rising rate worldwide [1]. Progressive cognitive decline is the typical clinical manifestation of AD, often accompanied by anxiety, depression, and other emotional disorders [2]. Especially in a considerable proportion of AD patients, depression symptoms emerge before cognitive impairments [3-6]. Therefore, exploring the common mechanisms of cognitive dysfunction and depressive behavior would benefit

the early diagnosis and treatment of AD.

Epigenetics plays an essential role in the pathogenesis of multiple diseases [7]. MicroRNAs (miRNAs) are a group of small noncoding RNAs that silence targeted genes at the post-transcriptional level [8]. Accumulated literature has shown the involvement of miRNAs in various neurological disorders, including AD [9] and depression [10]. Several miRNAs, such as miR-124, miR-135a, miR-132, miR-27a, and let-7, have been confirmed to be dysregulated in the brain tissue or serum of AD patients; and some of them are implicated in the accumulation of β-amyloid (Aβ) in AD transgenic mouse models [9, 11-14]. Notably, the serum levels of miR-132, miR-27a, let-7, miR-124, and miR-135a are also changed in patients with depression [15-19]. However, it remains to be elucidated which miRNAs are involved in AD patients coexisting with depression. Exploring this issue may benefit the early diagnosis and intervention of AD.

In the present study, we first screened for miRNAs associated with AD and depression from databases and literature. We identified an abnormal downregulation of miR-451a in the cerebrospinal fluid (CSF) of AD patients, and its levels correlated with cognition and depression scores. Consistently, miR-451a was also decreased in the medial prefrontal cortex (mPFC) of APP/PS1 transgenic mice. We further investigated whether overexpression of miR-451a in the mPFC rescued cognitive defects and depression-like symptoms of APP/PS1 mice. Finally, we addressed the potential mechanisms of miR-451a in regulating the pathogenesis of AD coexisting with depression.

Materials and Methods

Human samples

Human CSF samples were acquired from 47 participants, including 30 AD patients (48-76 years old) and 17 healthy volunteers (43-82 years old) who were recruited in the Affiliated Nanjing Brain Hospital of Nanjing Medical University (NMU) from March of 2019 to January of 2023 (Table S1-3). The recruitment of the AD patients was performed based on the current diagnostic criteria provided by the National Institute on Aging and the Alzheimer's Association Working Group (NIA-AA) in 2018. The guidelines are characterized by episodic memory loss in AD pathology supported by the evidence of CSF and imaging biomarkers [20]. Each CSF sample (1 mL) was collected with BD vacutainer tubes and stored at -80 ℃ till further processing. The Montreal Cognitive Assessment (MoCA) is a rapid screening tool for cognitive impairments in attention and concentration, executive functioning, memory, language, visuospatial skills, abstract thinking, and computational and orienting skills. The total MoCA score is 30. The individual who acquires MoCA score < 26 is diagnosed as having cognitive impairment [21]. The Hamilton Depression Scale (HAMD) is the most commonly used scale for clinically assessing depressive states. The scale is administered to patients by two trained raters in a combined HAMD examination, usually by talking and observing. A total score of less than 7 is rated as normal, and greater than 7 is assessed as the presence of depression [22]. The recruitment, specimen collection, clinical assessment, and testing protocols of all participants were approved by the Ethics Committee of Nanjing Brain Hospital Affiliated with NMU (Ethics number: 2019-KY033-02).

Animals

The male APP695/PS1-dE9 transgenic (APP/PS1) mice and wild-type (WT) littermates on a C57BL/6J background were purchased from Jackson Laboratories. All these mice were bred in the Experimental Animal Central of Nanjing Medical University. The mice were housed under a 12-h light/dark cycle in a temperature- and humidity-controlled environment with free access to food and water. Animal experiments were approved by the Institutional Animal Care and Use Committee of NMU (Approval No. IACUC-1812054).

Virus construction and stereotactic injection

Viral constructs with adeno-associated virus serotype 9 (AAV9) vectors encoded Ad_OE-miR-451a blending pri-mmu-miR-451a, and GFP protein (Genechem, China) was designed to induce overexpression of miR-451a, and Ad_OE-scramble with only GFP protein as a negative control virus controlled by the CMV promoter. Mice were anesthetized by intraperitoneal (i.p.) injection of pentobarbital sodium (40 mg/kg) and placed in a stereotaxic apparatus. A total volume of 0.25 μL of AAV-miR-451a-OE (2×10^{13} viral particles per mL) or control virus was injected into the bilateral mPFC (anteroposterior: + 1.90 mm, mediolateral: ± 0.5 mm, dorsoventral: - 2.3 mm relative to bregma) by use of 1 μL Hamilton microsyringe in an 8-min period. The infusion needles were left in place for 5 min to limit virus backflow. After the scalp was sutured, the mice were kept on a heating pad to recover until fully awake. Then, the mice were raised for four weeks, followed by behavioral tests.

Behavioral tests

Open field test

The open-field test assessed anxiety-like beha-

vior and exploratory activity [23]. The open field consisted of a plastic square blue box (60 × 60 × 25 cm) with an evident outlined center area (30 × 30 cm). Each mouse was placed in the middle of the box and allowed to explore the entire box freely for 5 min. The time spent in the central area and the number of central area entries during the test were recorded and analyzed.

Elevated plus maze test

Anxiety-like behavior was evaluated by the elevated plus maze test [24]. The apparatus consisted of an elevated (100 cm above the floor) plus-shaped platform with four intersecting arms (50 × 10 cm each): two opposing open arms and two closed arms with 15 cm high walls. The four arms were extended from a central platform (10 × 10 cm). Each mouse was placed in the center square facing the open arm and left to explore for 5 min freely. The time duration and entries in the open arm were calculated and analyzed.

Novel object recognition test

The novel object recognition test assessed short-term recognition memory in rodents [25]. This experiment used a rectangular box made of opaque plastic (50 × 35 cm) as the apparatus. Each mouse was placed in and allowed to habituate the apparatus for 5 min. Two identical plastic objects were placed on either corner of the box and 5 cm away from each adjacent arena wall. Each mouse was then placed in the arena and allowed to explore the arena and objects for 5 min. Two hours later, the mouse was again positioned in the same arena with one of the objects replaced with a novel object of a different shape and allowed to explore for another 5 min. A mouse was considered to be exploring an object when it was sniffing or touching it, and the time spent was measured. T1 represented the exploration time for the old object and T2 for the new object. The discrimination index was calculated as (T2-T1)/(T1+T2).

Y-maze test

Spatial memory was evaluated by the Y-maze test based on the nature of animals' spontaneous preference for spatial novelty [26]. The experiment consisted of two 5-min phases with a 2-hour interval. In the first phase, the novel arm was blocked by a black baffle, and mice were allowed to move freely only in the other two arms. The novel arm was opened in the second phase, and the mouse could freely move through all three arms. The percentage of time spent and number of entries in the novel arm were calculated.

Three-chamber test

Social ability was evaluated by the three-chamber test [27]. This test included the social preference test and social memory test. Mice were tested for social behavior in a chamber divided into three equal compartments (40 × 40 × 30 cm) by two square openings (8 × 8 cm) that allowed the test mice to enter. Before the social preference test, the mice were placed in the middle compartment and allowed to habituate for 5 min. In the social preference test, an unfamiliar male and age-matched mouse with the same background (stranger-1) was introduced into a mesh cage of one compartment. The testing mouse was then placed into the middle compartment and allowed to explore freely in the three compartments for 5 min. After a 10-min interval, the social memory test was conducted. Another age-matched stranger mouse (stranger-2) was introduced into the previously empty mesh cage. The testing mouse was again placed in the middle compartment and allowed to freely explore all three chambers for another 5 min. The percentage of time spent in each compartment was recorded.

Sucrose preference test

The sucrose preference test was operated to estimate the mouse anhedonia [28]. The mice were trained to drink from two drinking bottles and then were deprived of drinking water but had free to acquire food for 24 h before the test. Each mouse was housed in a single cage and given one pot of normal water and the other pot of 1% sucrose solution for 12 h. At the end of the first half of the testing period, the positions of two pots were switched to avoid side preference. Consumption of sucrose solution or water was estimated by weighing the bottles before and after the test. The sucrose preference was calculated as follows: Sucrose preference rate (%) = sucrose consumption/total solution consumption × 100%.

Forced swimming test

The forced swimming test was designed to evaluate depression-like behavior. The mice were exposed to an inescapable stressful environment (water), and their immobile time was recorded to assess their despairing behavior [29]. During the test, the mice were placed individually in a cylindrical glass cylinder (30 cm high, 10 cm in diameter) filled with 20 cm of water (24 °C). The duration of immobility of each mouse was analyzed during the last 4 min of the 5-min test.

Morris water maze

The Morris water maze was performed as previously described [30]. Briefly, markers of different shapes were pasted around the swimming tank, and the water was made opaque with milk at a temperature of 22 °C. The mice were trained to find

the hidden platform that submerged 1 cm beneath the water surface four times per day for six consecutive days. Once on the platform, the mice were allowed to remain on it for 15 s. If mice did not find the platform within 1 min, they were guided to the platform and allowed to stay for 15 s. On the seventh day, the hidden platform was removed; mice were placed in the quadrant opposite the target quadrant (previous location of the hidden platform) and allowed to swim for 1 min. The latency to reach the place of the platform, the percent time spent in the target quadrant, the crossing times to the platform regions, the swimming velocity, and the distance were recorded.

A digital video camera (Beijing Sunny Instruments Co. Ltd, China) connected to a computer was used to capture the activities of mice during the behavioral tests. The order of the behavioral tests was open field test (D30), elevated plus maze test (D31), novel objection recognition test (D32), Y-maze test (D33), three-chamber test (D34), sucrose preference test (D35), forced swimming test (D36) and Morris water maze (D37-D43). During the testing period, except for one dim light, all the lights in the room were turned off to ensure the comfort of the mice. At the end of each test, the mice returned to their home cages and rested for 24 hours. The experimental equipment was cleaned with 75% alcohol between each testing session to reduce cues that could affect trace and behavior. Two independent experimenters performed all tests, each blind to the treatment scheme.

Cell culture and labeling

Murine neuronal lines Neuro-2a (N2a) and human embryonic kidney cells (HEK293) cells were bought from the American Type Culture Collection (ATCC). Cells cultured in the Dulbecco's Modified Eagle's medium (DMEM) that was supplemented with 10% fetal bovine serum (FBS, Gibco Thermo Fisher, USA), 100 U/mL of penicillin and 100 µg/mL of streptomycin (Invitrogen, USA) at 37 °C with 5% CO_2.

Primary neuron cultures were prepared as previously described [31], the mPFC tissue was dissected out from postnatal day-1 WT and APP/PS1 mice and dissociated in DMEM containing dissociation buffer with 20-30 U/mL Papain (Sangon Biotech, China) and 2500 U DNase I (Sigma-Aldrich, USA) at 37 °C for 15 min, followed by FBS addition and 40 µm mesh filter to obtain dissociated cells. The suspension was centrifuged for 5 min at 1000 g and resuspended in neurobasal medium (Gibco) supplemented with 2% B27 (Gibco), 0.5 mmol/L glutamine (Sigma-Aldrich), and 1% penicillin/streptomycin (Gibco). Then, the cells were seeded into a poly-D-lysine (Sigma-Aldrich) precoated 6-well plates at a density of 5-10×10^6 cells/mL and cultured at 37 °C and 5% CO_2 for 24 h, then entirely replaced with culture medium. Finally, the culture medium was conducted a half-change every two days.

For primary microglial cultures [32], 1-day-old WT and APP/PS1 mice were decapitated, the mPFC was chopped with a 5 mL serological pipette, and the homogenates were obtained from spinning at 1000 g for 5 min. The supernatant was discarded, and the pellet was resuspended in a 10 mL pipette and drained through a 75 µm filter. The mPFC tissue was cultured in 75 cm^2 flasks in 15 mL of culture medium that contained DMEM with 10% FBS, 100 U/mL penicillin, and 100 µg/mL streptomycin at 37 °C with 5% CO_2. After 24 h, the new medium was added. The cultures were grown for an additional 10-14 days, and then the microglia were shaken from the astrocyte feeder layer for 2 h, resuspended in a culture medium, and plated.

For miR-451a knockdown, miR-451a inhibitors (RiboBio, Guangzhou, China) were used, and double-stranded miR-451a designed as mimic (RiboBio) to overexpress miR-451a. For toll-like receptor 4 (TLR4) downregulation, a double-stranded siRNA targeting mouse TLR4 or scrambled negative control (Shanghai GenePharma Co. Ltd, China) was used. For dual luciferase assays, the GV272 vector (GeneChem Biotechnology, Shanghai, China) was used, and the WT or mutation (Mut) 3′ UTR sequences of TLR4 are listed in Table S4. In short, N2a, HEK293, primary neurons, and primary microglial cells were plated in 12-well plates at 2 × 10^5 cells per well. After 24 h hatching, miR-451a mimic (50 nM), inhibitor (100 nM), or negative control (50 nM) were transfected with Lipofectamine 2000 (Invitrogen). The TLR4 siRNA (100 nM) and overexpression plasmid were transfected into cells according to the manufacturer's instructions. Cellular RNA, proteins, and fluorescence were obtained 48 h after transfection.

Immunofluorescence and fluorescence in situ hybridization (FISH)

Frozen brain sections were incubated with blocking buffer (5% bovine serum albumin, 0.3% PBS-Triton X-100) for 1 h at room temperature and then incubated with appropriate dilutions of primary antibodies (Table S5) overnight at 4 °C. After being washed with PBS for 3 times, brain sections were incubated with secondary immunofluorescence antibodies for 2 h at room temperature. After washed, brain sections were incubated with 1:1000 DAPI (4′, 6-diamidino-2-phenylindole) (Invitrogen; Cat. #D21490) diluted by PBS for 5 min at room

temperature. The sections were then washed with PBS and covered with glass coverslips. The images were captured using a confocal microscope (Zeiss LSM710, Germany).

The locked nucleic acid-modified miR-451a probes labeled with Cy3 were designed and constructed (Shanghai GenePharma Co. Ltd), and the probe sequence was AAC+TCAGTAA+TGGTAA CGGT+TT, "+" indicated the modification site of locked nucleotide. The probe signals were detected with a fluorescent in situ hybridization kit (RiboBio). In short, after pre-hybridization brain sections were incubated with miR-451a probes in hybridization solution at 37 °C overnight. The sections were washed with PBS and performed the immunofluorescent procedure described above. Two brain sections containing the mPFC or hippocampus were averaged for each mouse, and four to six mice were averaged for each group.

RNA extraction and analysis

The total RNA was isolated from human CSF, the mouse serum, mPFC, and hippocampus using RNAiso Plus (TAKARA, Japan) according to the manufacturer's protocols and quantified by Nanodrop 2000 (Thermo, USA). The detection of miRNA and mRNA was carried out in 96-well plates. Quantitative real-time PCR (qRT-PCR) was performed using an ABI 7300 Fast Real-Time PCR System (Applied Biosystems, USA).

Reverse transcription PCR for miRNAs was carried out using a Poly (A) tailing reaction and universal cDNA synthesis kit (Sangon Biotech Co., Ltd. Shanghai, China). Then the qRT-PCR was conducted using SYBR Green MicroRNAs qPCR Kit (B532461, Sangon Biotech, Shanghai, China). The small nucleolar RNA (snoRNA) RNU6B was used as endogenous controls for miRNA.

The mRNA was reverse transcripted using HiScript III RT SuperMix for qPCR (+gDNA wiper) (R323-01, Vazyme Biotech Co., Ltd, USA), and mRNA expression was assessed using a Taq Pro Universal SYBR qPCR Master Mix (Vazyme) by real-time PCR. Results were analyzed, presented relative to threshold cycle (CT) values, and then converted to fold changes. Glyceraldehyde-3-phosphate dehydrogenase (GAPDH) mRNA was used as an endogenous control. PCR was repeated at least twice for two separately prepared sets of samples. The expression of miRNAs and mRNAs was presented as fold change relative to control. The primer information is listed in Table S6.

Western blotting

For Western blot analyses, the homogenized protein samples of the brain and cells were loaded onto 8-15% Tris/tricine SDS gels and electrophoretically transferred to PVDF membranes (Millipore, USA). After blocking for 1 h in 5% nonfat milk/TBST, the membranes were incubated at 4 °C overnight with primary antibodies (Table S5). The membranes were then incubated with horseradish peroxidase-conjugated secondary antibodies (1:2000; Vector Laboratories, USA) for 1 h at room temperature. Blots were visualized using an ECL kit (Tanon, Shanghai, China). Westerns blots were quantified using ImageJ software (NIH, USA) using an internal GAPDH loading control for each blot analyzed. Fold changes in expression were calculated relative to the control group. The experiments were repeated at least twice for each sample, and six mice in each group were used for statistical analysis.

Enzyme-linked immunosorbent assay (ELISA)

For ELISA of interleukin-1β (IL-1β), interleukin-6 (IL-6), tumor necrosis factor-α (TNF-α), soluble $A\beta_{1-40}$, and $A\beta_{1-42}$ concentrations, mPFC tissues and primary neuron cells were homogenized in lysis buffer with protease inhibitors. After mixed, samples were centrifuged at 12,000 g for 20 min, and the supernatant was measured with ELISA kits ($A\beta_{1-40}$ and $A\beta_{1-42}$ purchased from Jingmei Bio, Shenzhen, China; IL-1β, IL-6, and TNF-α purchased from ExCell Bio, Shanghai, China) according to the manufacturer's protocols. All samples were tested at least twice.

β-site APP cleaving enzyme 1 (BACE1) activity analysis

BACE1 enzyme activity detection was performed according to the manufacturer's instructions (β-Secretase Activity Fluorometric Assay Kit, Sigma-Aldrich). Briefly, the lysis buffer of the primary cells was centrifuged at 10,000 g for 5 min, and a portion was used for the quantitative protein experiment with the BCA method. Then 50 μL of cell lysis was added, followed by the addition of reaction buffer and substrate. Fluorescence for each sample was measured using the full-wavelength microplate reader. The analyses were repeated at least twice in all samples.

Statistical analysis

Statistical tests for each figure were justified to be appropriate using Prism 8.0 (GraphPad Software, Inc.). Data are presented as mean ± SEM. Two-tailed unpaired student's *t*-tests were utilized for comparisons between two groups, and one-way ANOVA was used to compare three independent groups. Multifactorial comparisons were analyzed by two-way ANOVA with Tukey's post-hoc test. Pearson's correlation analysis was conducted to

evaluate the correlation between CSF miR-451a levels and indicators of AD patients. Significance was determined as p values < 0.05.

Results

CSF miR-451a levels in AD patients were positively correlated with MoCA score and negatively correlated with HAMD score

To explore the potential role of miRNAs in the comorbidity of AD and depression, both AD and depression-related miRNAs were screened from the literature [33-35], database GSE157239 of AD, and GSE81152 and GSE58105 of depression. Nine miRNAs including miR-30a-5p, miR-345, miR-375, miR-451a, miR-4726-3p, miR-765, miR-1257, miR-486-5p, and miR-320e were successfully screened out (Figure 1A). The expression levels of these nine miRNAs in the CSF samples of AD patients and healthy volunteers were further validated by qRT-PCR. Only four miRNAs, including miR-30a-5p, miR-486-5p, miR-320e, and miR-451a, changed in AD patients, compared with healthy controls (Figure 1B). The correlation between the four miRNAs and cognitive score or depression severity in AD patients was further analyzed. The results showed that the miR-451a levels were positively correlated with the MoCA score but negatively with the HAMD score (Figure 1C, D). Furthermore, the CSF levels of miR-451a were lower in AD patients with depressive symptoms than in AD patients without depression (Figure S1A). The miR-320e levels were positively correlated with the MoCA score (Figure 1C), and the miR-1257 levels were negatively correlated with the HAMD score (Figure S2B). Otherwise, the associations between the other six miRNA levels and MoCA or HAMD were not observed (Figure S2A, B). After exclusion of confounding factors including gender and age in four changed miRNAs, the miR-451a levels were positively correlated with $A\beta_{1-40}$ levels (Figure 1E), and the miR-30a-5p levels were negatively correlated with total Tau levels in the CSF (Figure S3A). Moreover, we did not observe any associations between miR-486-5p, miR-320e levels and indicators of AD patients including age, gender, Aβ levels ($A\beta_{1-42}$, $A\beta_{1-40}$, and $A\beta_{1-42}/A\beta_{1-40}$), and Tau levels (total Tau and p-Tau) (Figure S3B, C). We also analyzed miR-451a levels of Early-Onset AD (EOAD, age < 65) and Late-Onset AD (LOAD, age ≥ 65) and did not find significance between the two groups (Figure S1B). Based on this, we focused on exploring the potential involvement of miR-451a in the co-pathogenesis of AD and depression using APP/PS1 double transgenic mouse model for AD.

Decreased miR-451a levels in the CSF and mPFC of APP/PS1 mice

Serum miR-451a levels in APP/PS1 transgenic mice were examined at ages 3, 5, 7, and 9 months and decreased from 7 months compared to age-matched controls (Figure S4A). Previous studies have reported that miR-451a is enriched in the brain and participates in glioma cell invasiveness [36], neuroinflammation, oxidative stress [37], and neuronal apoptosis [38]. The dynamic changes of miR-451a in the hippocampus and mPFC, two brain regions markedly impacted in AD or depression, were investigated [39-41]. Also, at 7 and 9 months old, the levels of miR-451a decreased significantly in the mPFC of APP/PS1 mice (Figure S4B). However, its expression in the hippocampus was similar between APP/PS1 and WT mice in the above age groups (Figure S4C). Decreased miR-451a levels were also observed in the CSF of 7-month-old APP/PS1 mice (Figure S4D, E). The fluorescence in situ hybridization confirmed a decrease in miR-451a expression in the mPFC of the 7-month-old APP/PS1 mice (Figure 2A, F). Double staining revealed that miR-451a was localized in both NeuN positive neurons (Figure 2B, C) and ionized calcium-binding adapter molecule 1 (IBA1) positive microglia (Figure 2D, E) in the mPFC, which dramatically reduced in APP/PS1 mice (Figure 2H, I). The levels of miR-451a were extremely low in the hippocampus, and there was no significant difference between the two genotypes of mice (Figure 2A, G).

Overexpression of miR-451a in the mPFC alleviated long-term spatial memory and depression-like behavior in APP/PS1 mice

Previous studies, including those from our group, demonstrated that apart from age-dependent cognitive defects, APP/PS1 mice also exhibit depression-like behavior [42, 43]. To investigate whether miR-451a was involved in these abnormal behaviors, AAV9-miR-451a-GFP or control virus (AAV9-scramble-GFP) were injected into the mPFC of APP/PS1 mice at 7 months to induce and measure the miR-451a overexpression of WT and APP/PS1 mice. Four weeks later, a series of behavioral tests were performed (Figure 3 A, B). As expected, AAV9-miR-451a-GFP injection in the mPFC of APP/PS1 mice upregulated miR-451a gene levels by 3-4 folds compared with the AAV9-scramble-GFP control group, as shown by qRT-PCR (Figure 3C).

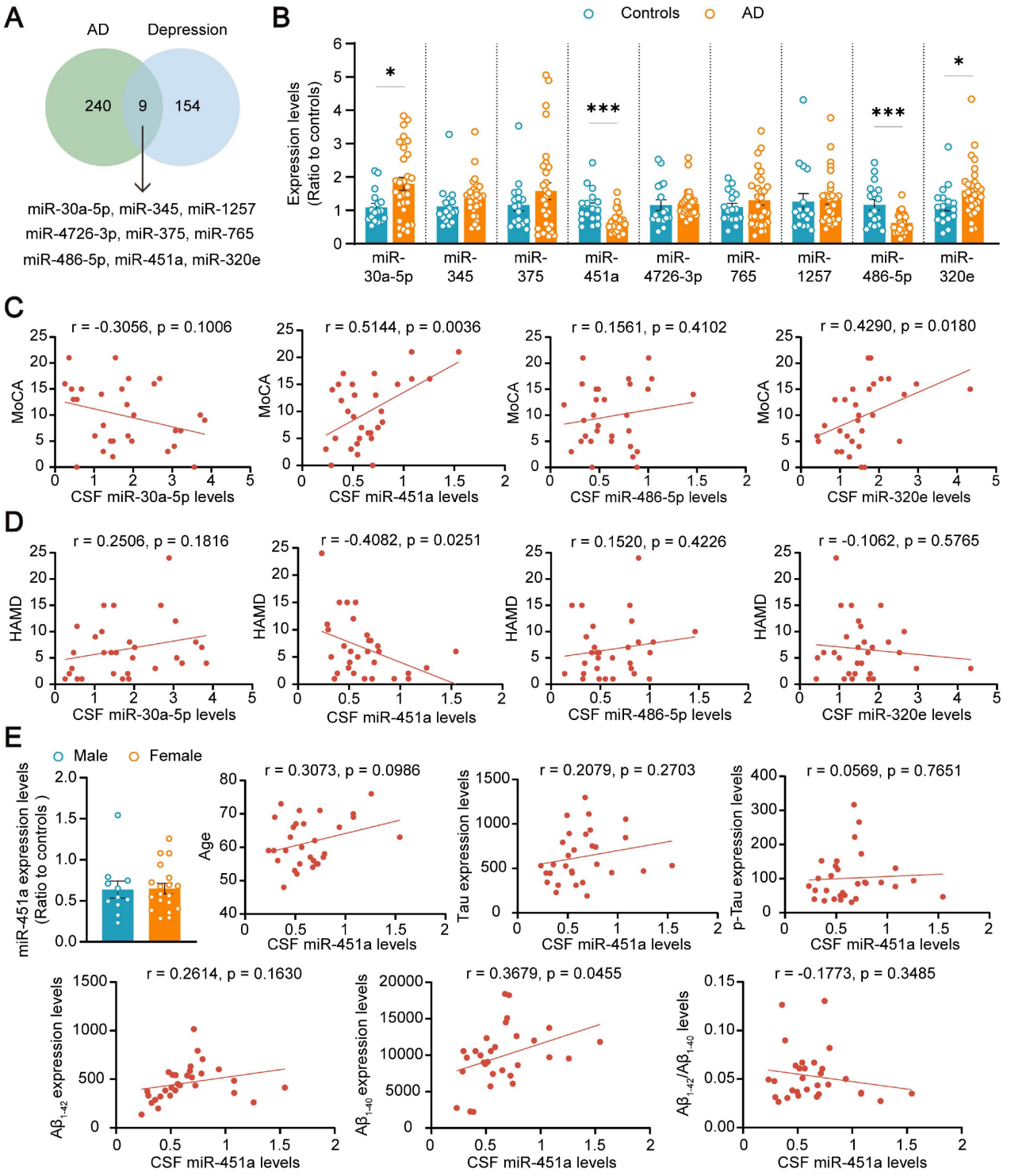

Figure 1. MiR-451a is altered in AD patients. (A) The results of database search and screening. Nine miRNAs were screened out by multiple literature and GEO databases of AD and Depression. **(B)** qRT-PCR evaluating the levels of miR-30a-5p, miR-345, miR-375, miR-451a, miR-4726-3p, miR-765, miR-1257, miR-486-5p, and miR-320e in the CSF of AD patients and control individuals. **(C)** Correlation analysis between the relative CSF levels of miR-30a-5p, miR-451a, miR-486-5p, and miR-320e in AD patients and the total score of MoCA, respectively. **(D)** Correlation analysis between the relative CSF levels of each miRNA mentioned above in AD patients and the total score of HAMD. **(E)** Analysis of the relationship between CSF miR-451a levels and gender, age, Aβ levels, and Tau levels, respectively. Data are presented as mean ± SEM. n = 30 for AD patients (11 males and 19 females) and n = 17 for controls (11 males and 6 females). Significance was evaluated with Student's *t*-test (**B, E**) or Pearson's correlation test (**C, D, E**). **p* < 0.05, ****p* < 0.001.

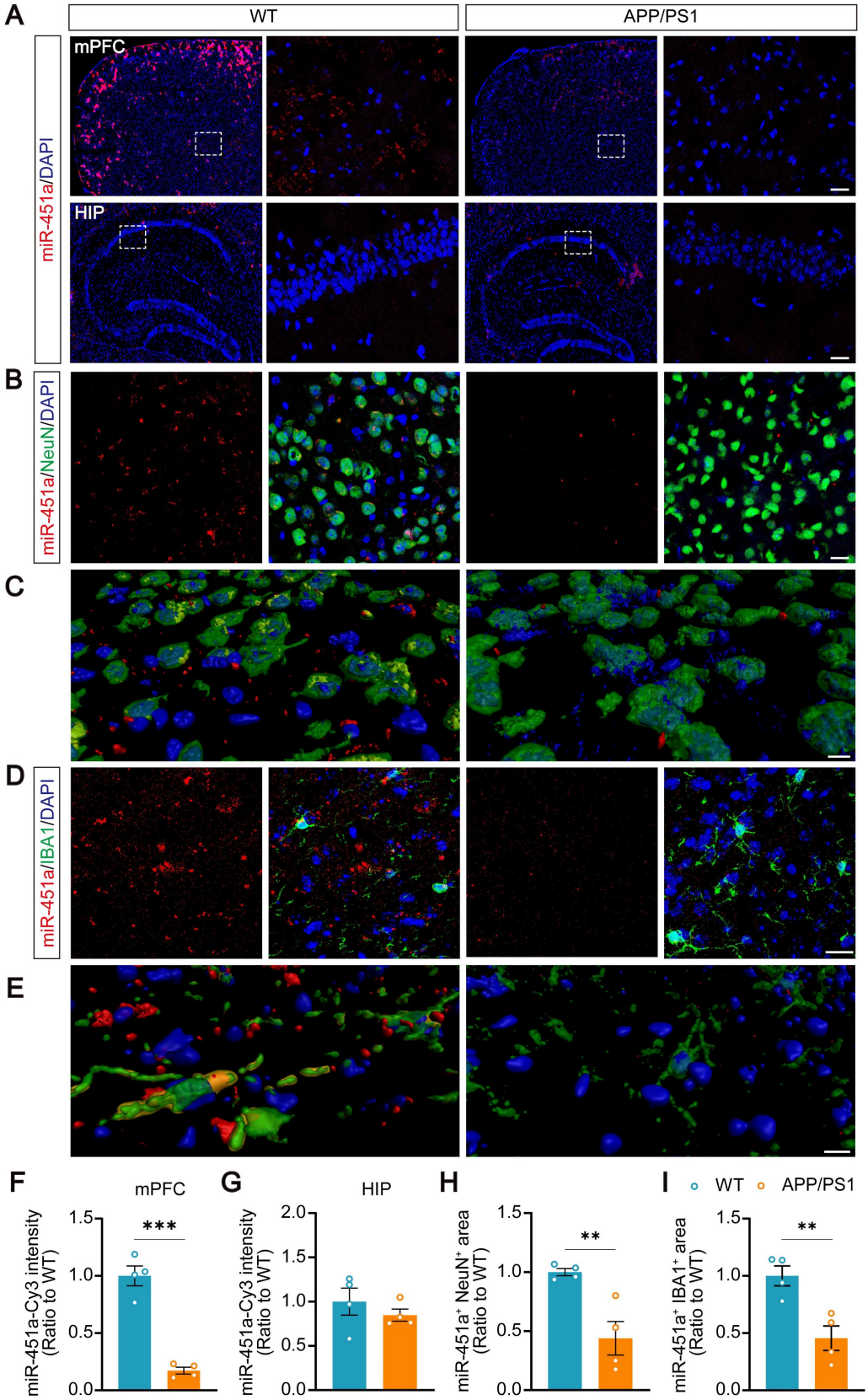

Figure 2. Decreased expression of miR-451a in the mPFC neurons and microglia in APP/PS1 mice. (A) Representative RNA FISH images showed decreased miR-451a expression in the mPFC (upper panel) but not in the hippocampus (lower panel) of 7-month-old APP/PS1 mice compared to age-matched WT mice. Scale bar, 20 μm. **(B)** Representative imaging showed that miR-451a was partially colocalized within NeuN positive neurons and down-regulated expression in APP/PS1 mice, compared with WT mice. Scale bar, 20 μm. **(C)** Three-dimensional reconstruction and surface rendering for FISH of miR-451a within neurons. Red showed outside cells, and yellow showed inside cells. Scale bar, 10 μm. **(D)** A small proportion of miR-451a was also expressed in the IBA1-positive microglia and significantly down-regulated in APP/PS1 mice. Scale bar, 20 μm. **(E)** Three-dimensional reconstruction and surface rendering for FISH of miR-451a in microglia. Red showed outside cells, and yellow showed inside cells. Scale bar, 10 μm. **(F)** The fluorescence intensity of miR-451a in the mPFC. **(G)** The fluorescence intensity of miR-451a in the hippocampus (HIP). **(H)** The relative area percentage of miR-451a and

NeuN double-positive signals in the mPFC. **(I)** The relative area percentage of miR-451a and IBA1 double-positive signals in the mPFC. Data are presented as mean ± SEM. n = 4 per group. Significance was evaluated with Student's *t*-test. ***p* < 0.01, ****p* < 0.001.

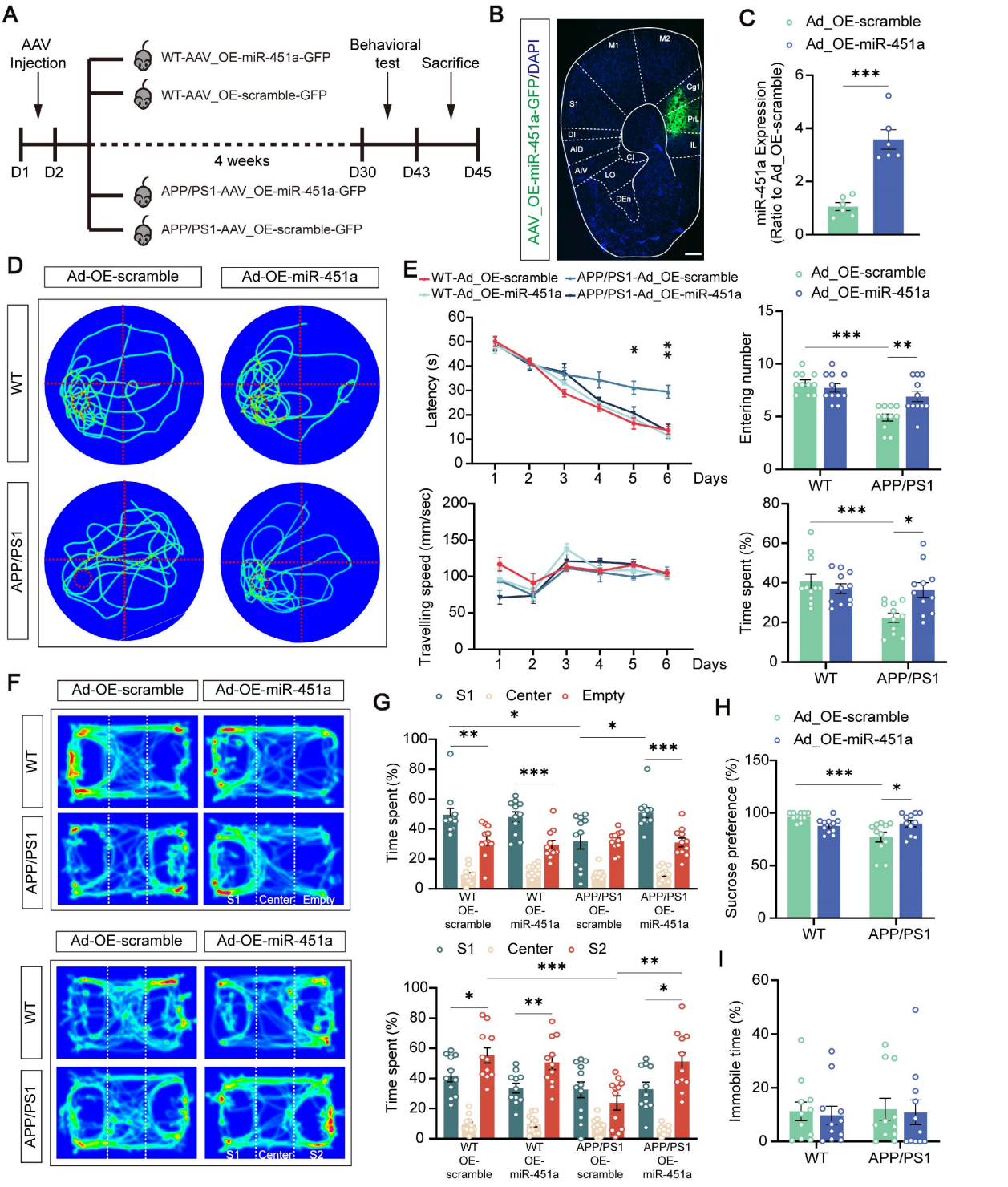

Figure 3. Overexpression of miR-451a rescued behavior alterations in APP/PS1 mice. (A) Schematic diagram illustrating experimental time course for APP/PS1 and WT mice that underwent AAV injection, behavioral tests, and sacrifices (OE-miR-451a for miR-451a overexpression and OE-scramble for a negative control). **(B)** The representative fluorescence image of the AAV virus-infected slice. Scale bar, 400 μm. IL: infralimbic cortex; PrL: prelimbic cortex; Cg1: cingulate cortex, area 1; M2: secondary motor cortex; M1: primary motor cortex; S1: primary somatosensory cortex; DI: dysgranular insular cortex; AID: agranular insular cortex, dorsal part; AIV: agranular insular cortex, ventral part; CI: caudal interstitial; LO: lateral orbital cortex; DEn: dorsal endopiriform nucleus. **(C)** Injection of AAV_OE-miR-451a-GFP increased miR-451a level in the mPFC of APP/PS1 mice, as revealed by qRT-PCR results. **(D)** Traces on the probe trial on day 7 in the Morris water maze. **(E)** The latencies to the target quadrant containing platforms, swimming speed, entering time, and time spent in the target quadrant in the Morris water maze. **(F)** Track of mice in the three-chamber sociability test, including social preference test and social memory test. **(G)** The percentage of interaction time spent in three chambers in the social preference test (S1: Stranger mice 1) and social memory test (S2: Stranger mice 2). **(H)** Quantification of sucrose intake preference in the sucrose preference test. **(I)** Quantification of immobility time in the forced swimming test. Data are presented as mean ± SEM. n = 6 per group for **(C)** and n = 11 per group for (**E, G, H, I**). Significance was evaluated with Student's *t*-test (**C**), two-way ANOVA with Tukey post- hoc test (**E, G, H, I**), repeated two-way measures ANOVA with Tukey post-hoc test (latency and speed in **E**), or one-way ANOVA with Tukey post-hoc test (comparison within group in **G**). **p* < 0.05, ***p* < 0.01, ****p* < 0.001.

In the Morris test for long-term spatial memory, such virus-induced miR-451a overexpressed APP/PS1 mice showed a significantly shortened latency to find the hidden platform during the training phase (Figure 3D) and crossed the target quadrant more often and spent more time in the quadrant in which the platform was located during the probe test compared with the AAV9-scramble-GFP injected control group (Figure 3E). However, such improved memory benefits by miR-451a overexpression failed to be observed during the Y maze and novel objection recognition short-term memory test (Figure S5A-D). In addition, miR-451a upregulation partially rescued the decreased sucrose preference (Figure 3H) and social preference and social memory in the three-chamber test (Figure 3F, G), without affecting immobility time in the forced swimming test (Figure 3I) or anxiety-like performance in the open field and elevated plus maze of the APP/PS1 mice (Figure S5E-H). Taken together, these results demonstrated that overexpression of miR-451a in the mPFC specifically alleviated the impaired long-term spatial memory and depressive-like behavior of APP/PS1 mice.

Overexpression of miR-451a ameliorated AD neuropathology in the mPFC of APP/PS1 mice

To investigate the involvement of miR-451a in AD-like pathology of APP/PS1 mice, Aβ metabolism, plaque deposition, and glial activation in the mPFC and hippocampus were examined. Our results demonstrated that AAV9-miR-451a-GFP treatment significantly reduced thioflavine-S-positive Aβ plaques in the mPFC rather than hippocampus of APP/PS1 mice (Figure 4A, C). Consistently, immunofluorescence of 6E10-positive plaques also confirmed the result (Figure 4B, D). Moreover, overexpression of miR-451a decreased soluble $A\beta_{1-40}$ and $A\beta_{1-42}$ levels in the mPFC of APP/PS1 mice (Figure 4E). In addition, miR-451a overexpression successfully rescued pathologically increased β-secretase metabolites of APP, including Aβ monomer, oligomers, and β-C-terminal fragment (CTF-β) and its key regulator, beta APP cleaving enzyme 1 (BACE1) in the mPFC of such AD model mice (Figure 4F-I). However, no other regulators were affected by miR-451a overexpression (Figure 4H, I). Further, immunofluorescence confirmed a down-regulated BACE1 expression in the mPFC rather than hippocampus of miR-451a overexpressed APP/PS1 mice (Figure S6A-F). Our results proposed that miR-451a overexpression in the mPFC of APP/PS1 mice could alleviate the AD pathology of APP/PS1 mice by specifically targeting BACE1 to counteract the deleterious β-secretase metabolites of APP.

MiR-451a down-regulated BACE1 through targeting TLR4/IKKβ/NF-κB signal pathway

It is well-known that miRNAs regulate gene expression by inhibiting the gene's translation or enhancing the degradation of their target mRNAs [44]. Therefore, in the next *in vitro* experiments, the miR-451a mimic was used to determine how miR-451a regulated BACE1 expression. The transfection of miR-451a mimic induced a significant increase of miR-451a and a substantial decrease of BACE1 mRNA expression in 293T cells (Figure 5B, C). In primary cortical neurons, miR-451a mimic also successfully decreased activity of the BACE1 enzyme (Figure 5A), which further confirmed the regulation of BACE1 by miR-451a.

However, the results analyzed by the Targetscan and miRanda databases showed that BACE1 was not a direct downstream target of miR-451a (Figure 5E). Therefore, 11 potential downstream targets of miR-451a, including transcription factor 2 (ATF2), Friend leukemia integration 1 (FLI1), myelocytomatosis oncogene (MYC), nuclear factor I/B (NFIB), peroxisome proliferative activated receptor gamma co-activator 1 alpha (PPARGC1A), sine oculis homeobox 1 (Six1), T-box 19 (Tbx19), toll-like receptor 4 (TLR4), WW domain containing transcription regulator 1 (WWTR1), Y box protein 1 (YBX1), and zinc finger protein of the cerebellum 3 (Zic3) were screened out by TRRUST and analyzed (Figure 5D). Among the 11 candidates, only FLI1, TLR4, and WWTR1 showed increased mRNA levels in the mPFC of APP/PS1 mice (Figure S7A). After miR-451a overexpression, only the TLR4 level was normalized in this AD model mice (Figure S7B). Further investigation via bioinformatics analysis of the GSE33000 dataset of mPFC in AD patients downloaded from the GEO database supported the forementioned findings, showing that the expression level of TLR4 was increased in the mPFC of AD patients (Figure S7C). Thus, miR-451a may target BACE1 by directly regulating the TLR4.

It has been shown that NF-κB/P65 could specifically interact with their binding element in the BACE1 promoter regions [45]. In agreement with this, we found that overexpression of miR-451a decreased the activation of TLR4/IKKβ/NF-κB signal pathway in the mPFC of APP/PS1 mice (Figure 5F, G). To further explore whether miR-451a could regulate BACE1 expression by inactivating TLR4/IKKβ/NF-κB pathway, TLR4 siRNA was used to block the translation of TLR4 in the N2a cells. As expected, TLR4 siRNA markedly reduced mRNA levels of TLR4 (Figure 5H) and protein levels of TLR4, p-IKKβ, p-NF-κB, and BACE1 in N2a cells (Figure 5I, J). Then, TLR4 overexpression plasmid-treated N2a cells

showed a significantly elevated mRNA level of TLR4 (Figure 5K) and counteracted miR-451a mimic-induced protein decline of TLR4 and BACE1 (Figure 5L, M).

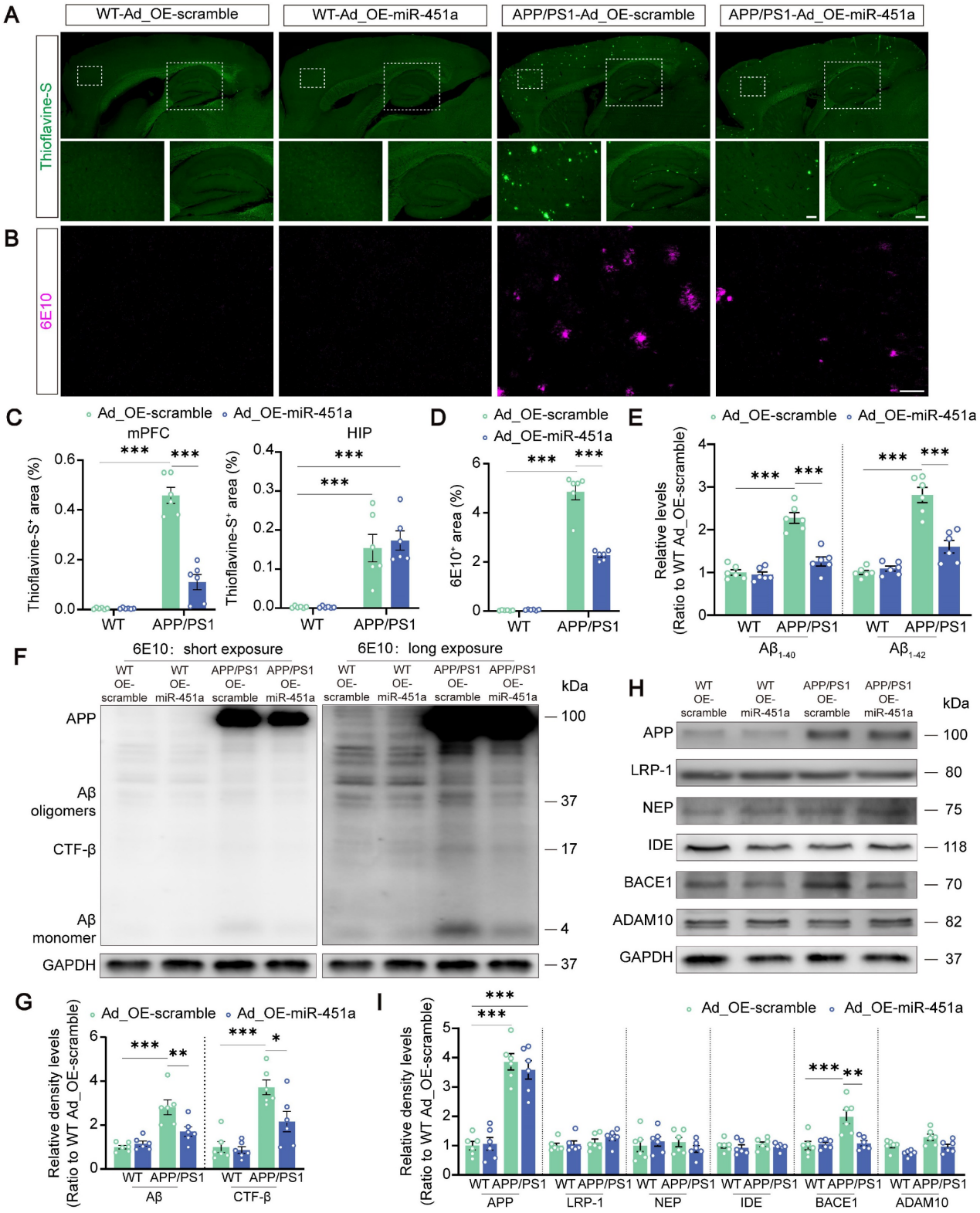

Figure 4. Overexpression of miR-451a ameliorated Aβ load and inhibited BACE1 expression in the mPFC of APP/PS1 mice. (A) Representative images of thioflavine-S$^+$ plaques in the mPFC and hippocampus of each group. Scale bar, 20 μm for the mPFC and 50 μm for the hippocampus (HIP), respectively. **(B)** Representative image of 6E10$^+$ plaques in the mPFC of each group. Scale bar, 50 μm. **(C)** The percentage of thioflavine-S$^+$ area in the mPFC and hippocampus, respectively. **(D)** The percentage of 6E10$^+$ area in the mPFC. **(E)** ELISA analyses of soluble A$\beta_{1\text{-}40}$ levels and A$\beta_{1\text{-}42}$ levels in the mPFC of each group. **(F, G)** Representative Western blot bands and densitometry analysis for Aβ and CTF-β in the mPFC of each group. **(H, I)** Representative Western blot bands and densitometry analysis for APP, LRP-1, NEP, IDE, ADAM10, and BACE1 in the mPFC of each group. Data are presented as mean ± SEM. n = 6 per group. Significance was evaluated with two-way ANOVA with Tukey post-hoc test. *$p < 0.05$, **$p < 0.01$, ***$p < 0.001$.

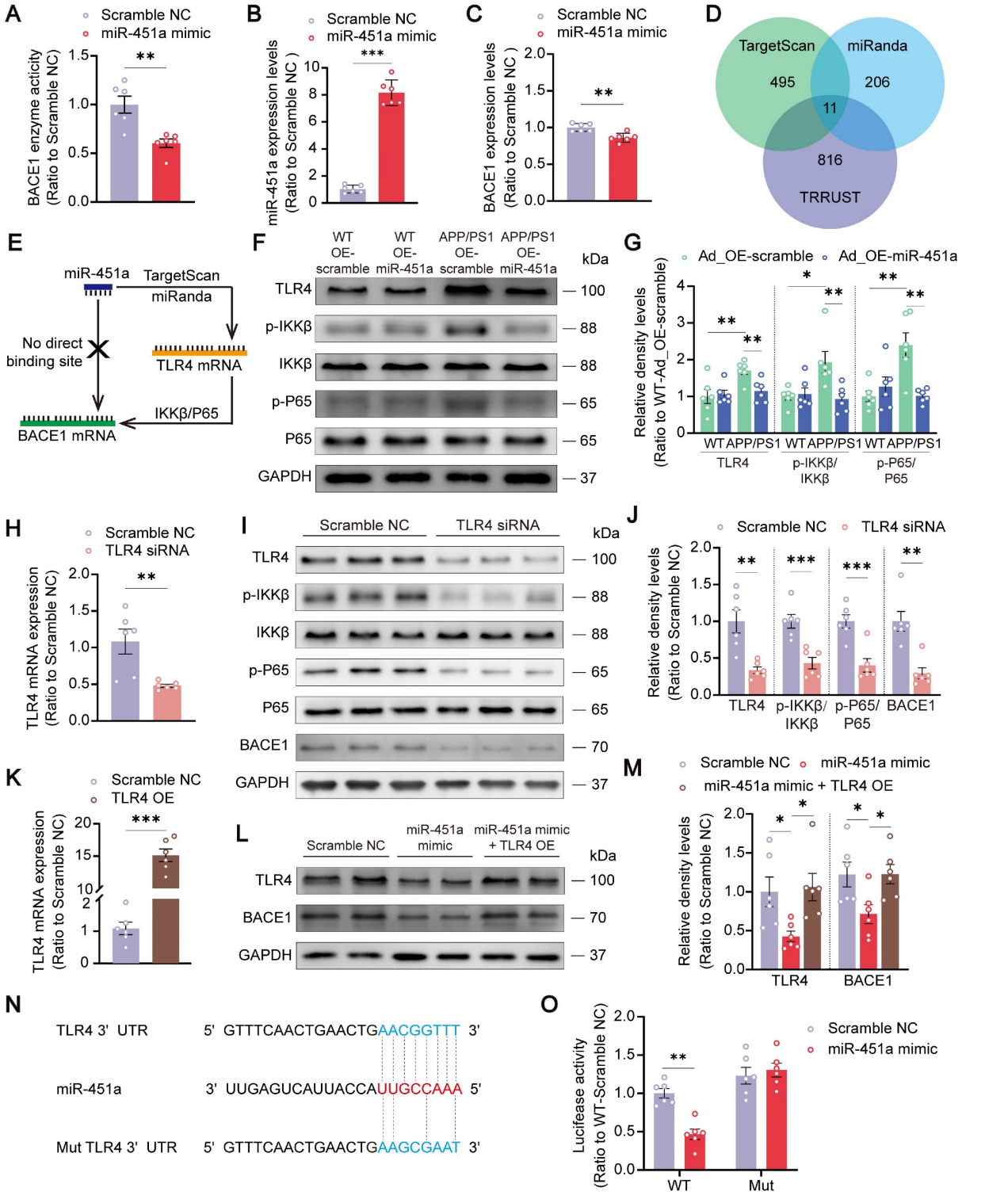

Figure 5. MiR-451a downregulated BACE1 transcription by targeting TLR4/IKKβ/NF-κB signal pathway. (A) The activity of BACE1 enzyme in primary cortical neurons after miR-451a mimic treatment. **(B)** qRT-PCR showed that miR-451a expression was significantly up-regulated in 293T cells after miR-451a mimic (50 nM) treatment. **(C)** qRT-PCR showed that BACE1 mRNA levels were prominently decreased in 293T cells after miR-451a mimic (50 nM) treatment. **(D)** A Venn diagram showing transcription factors (816 genes) from TRRUST overlapped with the target genes of miR-451a predicted by miRanda (206 genes) or TargetScan (495 genes). **(E)** The direct targets of miR-451a predicted by TargetScan and miRanda did not include BACE1 but include TLR4, which mediated IKKβ/NF-κB pathway to downregulate BACE1 production. **(F, G)** Representative Western blot bands and densitometry analysis for TLR4/IKKβ/NF-κB pathway-related proteins showed that overexpression of miR-451a reduced TLR4 expression, p-IKKβ/IKKβ and p-P65/P65 in the mPFC of APP/PS1 mice. **(H)** qRT-PCR showed that TLR4 siRNA (100 nM) reduced the mRNA levels of TLR4 in N2a cells. **(I, J)** Representative Western blot bands and densitometry analysis showed that TLR4 siRNA (100 nM) reduced the levels of TLR4, p-IKKβ/IKKβ, p-NF-κB/NF-κB and BACE1 in N2a cells. **(K)** qRT-PCR showed that overexpression of TLR4 increased the mRNA levels of TLR4 in N2a cells. **(L, M)** Representative Western blot bands and densitometry analysis showed that miR-451a mimic reduced the protein levels of TLR4 and BACE1, and overexpression of TLR4 normalized the levels of these proteins in N2a cells. **(N)** The sequence analysis indicated the nucleotide base pairing of the miR-451a binding region in TLR4 3'UTR. The mutant sequence of TLR4 3'UTR for luciferase analysis was provided at the bottom. **(O)** The quantification of luciferase reporter assays of WT and Mut sequence of TLR4 3'UTR in 293T cell after treatment of miR-451a mimic. Data are presented as mean ± SEM. n = 6 per group. Significance was evaluated with Student's *t*-test (**A, B, C, H, J, K**), two-way ANOVA with Tukey post-hoc test (**G, O**), or one-way ANOVA with Tukey post-hoc test (**M**). *$p < 0.05$, **$p < 0.01$, ***$p < 0.001$.

Moreover, the miR-451a inhibitor increased the activation of TLR4/IKKβ/NF-κB signal pathway in N2a cells (Figure S7D, E). To demonstrate the direct regulation of TLR4 by miR-451a, we constructed the WT 3′UTR region of TLR4, which contains the miR-451a binding site, and a 3′UTR mutation with a variant at the miR-451a binding site. Then, we subcloned them in the GV272 vectors and transfected them into 293T cells with either the miR-451a mimic or scrambled control. The WT and Mut 3′UTR sequences of TLR4 were listed in Table S4. We found that the miR-451a mimic suppressed the luciferase intensity in cells transfected with the WT construct but not the mutated construct (Figure 5N, O).

MiR-451a alleviated neuroinflammation via inhibiting NLRP3 activation in microglia

Neuroinflammation is confirmed as a common pathogenic manifestation of AD and depression [46, 47], in which miRNAs play a non-negligible role [48]. As mentioned above, miR-451a was also down-regulated in mPFC microglia of APP/PS1 mice (Figure 2D). Therefore, we examined its role in reactive gliosis and found that overexpression of miR-451a reduced activated microglia and astrocytes with decreasing of Aβ plaques in the mPFC of APP/PS1 mice, as revealed by a low percentage area of IBA1, GFAP and 6E10 immunostaining (Figure 6A, B), but no significant difference in the hippocampus (Figure S8A-D). Moreover, AAV9-miR-451a-GFP-induced miR-451a overexpressed APP/PS1 mice had low levels of inflammatory cytokines, including IL-1β, IL-6, and TNF-α (Figure 6C). Recently, it has been reported that miR-451a relieves chronic inflammatory pain by inhibiting microglia activation-mediated inflammation [49] and suppressing NLRP3-induced proinflammatory cascade signaling [50]. Consistently, our results revealed that miR-451a overexpressed APP/PS1 mice had decreased NLRP3 expression on the microglia (Figure 7A, B) as well as its downstream effectors ASC and Caspase-1 in the mPFC (Figure 7C, D). In *vitro*, miR-451a mimic also down-regulated NLRP3/ASC/Caspase-1 signal pathway in the primary microglia from APP/PS1 mice (Figure 7E, F).

MiR-451a protected primary neurons from APP/PS1 mice

Previous literature suggested that neuronal degeneration occurred in the cerebral cortex of APP/PS1 mice, and the neurons were prone to atrophy when cultured *in vitro* [51-54]. Our results consistently showed that primary cortical neurons derived from newborn APP/PS1 mice had significantly decreased length and number of neuritic branches compared with those from WT mice. MiR-451a mimic remarkably rescued neuronal degeneration in culture (Figure 8A, B). In addition, miR-451a mimic significantly rescued synaptic protein loss of APP/PS1 mice in *vivo* and *vitro* (Figure S9A-D). Moreover, miR-451a mimic decreased $A\beta_{1-40}$ and $A\beta_{1-42}$ deposition in primary neurons from APP/PS1 mice. Supernatant centrifuged from primary neurons in APP/PS1 mice with the treatment of miR-451a mimic produced less $A\beta_{1-40}$ rather than $A\beta_{1-42}$ (Figure S10A, B). Our results also showed that BACE1 and downstream products, such as sAPPβ and CTF-β, increased in primary neurons from APP/PS1 mice and decreased with treatment of miR-451a mimic (Figure S10C, D). As discussed earlier in the previous section, miR-451a could modulate TLR4 to reduce the production of Aβ in the mPFC of APP/PS1 mice. Therefore, we explored whether the dendritic protective effect from miR-451a was caused by TLR4 inhibition. TLR4 mRNA levels were blocked by siRNA to examine BACE1 expression and Aβ production in the primary neurons. Our results showed that TLR4 siRNA caused a decrease in $A\beta_{1-42}$ levels but failed to influence $A\beta_{1-40}$ contents within primary neurons from APP/PS1 mice. Supernatant centrifuged from primary neuronal medium showed less $A\beta_{1-40}$ and $A\beta_{1-42}$ concentrations after treatment of TLR4 siRNA (Figure S10E, F). Moreover, we found that BACE1, sAPPβ, and CTF-β increased in primary neurons from APP/PS1 mice and decreased with the treatment of TLR4 siRNA (Figure S10G, H). Interestingly, we found that TLR4 siRNA rescued neuronal atrophy (Figure 8C, D). The above results demonstrated that TLR4 modulated by miR-451a produced a protective effect for primary neurons from APP/PS1 mice.

Discussion

Clinical research shows that 50% of AD patients are accompanied by depression, which is also the leading risk factor in AD [55, 56]. Therefore, it is necessary to explore the co-pathogenesis of AD and depression. As an essential component of epigenetics, miRNAs have attracted more attention in neuro-psychiatric diseases, including AD [57, 58]. In this study, we screened nine miRNAs involved in both AD and depression. Changes of these nine miRNAs in AD or/and depression according as previous literature were summarized in Table S7.

Consistent with the previous literature [59-61], we verified the changes of these nine miRNAs in the CSF of AD patients and found that miR-30a-5p and miR-320e levels increased. In contrast, miR-486-5p and miR-451a levels decreased compared to those in age-matched controls. However, few studies addressed the correlation between CSF miRNA levels

and cognitive dysfunction or depressive behavior in AD cases. In this study, we conducted the correlation analysis and found that only CSF miR-451a levels were related to both MoCA and HAMD scales, indicating an involvement in the co-pathogenesis of AD and depression. Interestingly, we also found that CSF miR-451a levels were lower in depressed AD patients than in AD patients without depression, suggesting that miR-451a may be an essential regulatory molecule for depressive symptoms in AD.

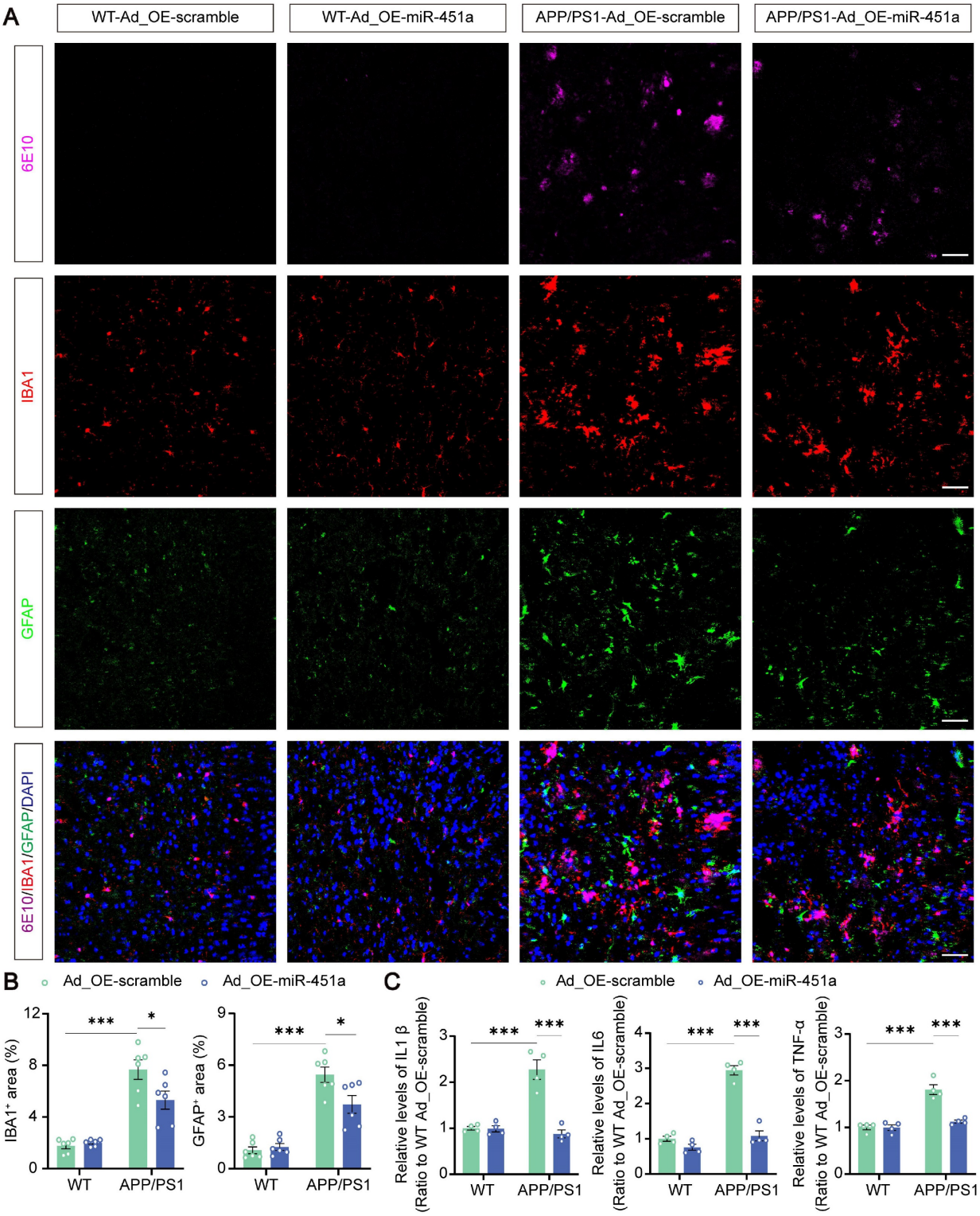

Figure 6. MiR-451a inhibited neuroinflammation in the mPFC of APP/PS1 mice. (A) Representative image of 6E10 (Magenta), IBA1 (Red), GFAP (Green), and DAPI (Blue) in the mPFC of each group. Scale bar, 50 μm. **(B)** The percentage of IBA1⁺ and GFAP⁺ area in the mPFC. **(C)** ELISA analyses of IL-6, IL-1β, and TNF-α levels in the mPFC of each group. Data are presented as mean ± SEM. n = 6 per group for (**B**) and n = 4 per group for (**C**). Significance was evaluated with two-way ANOVA with Tukey post-hoc test. **p* <0.05, ****p* < 0.001.

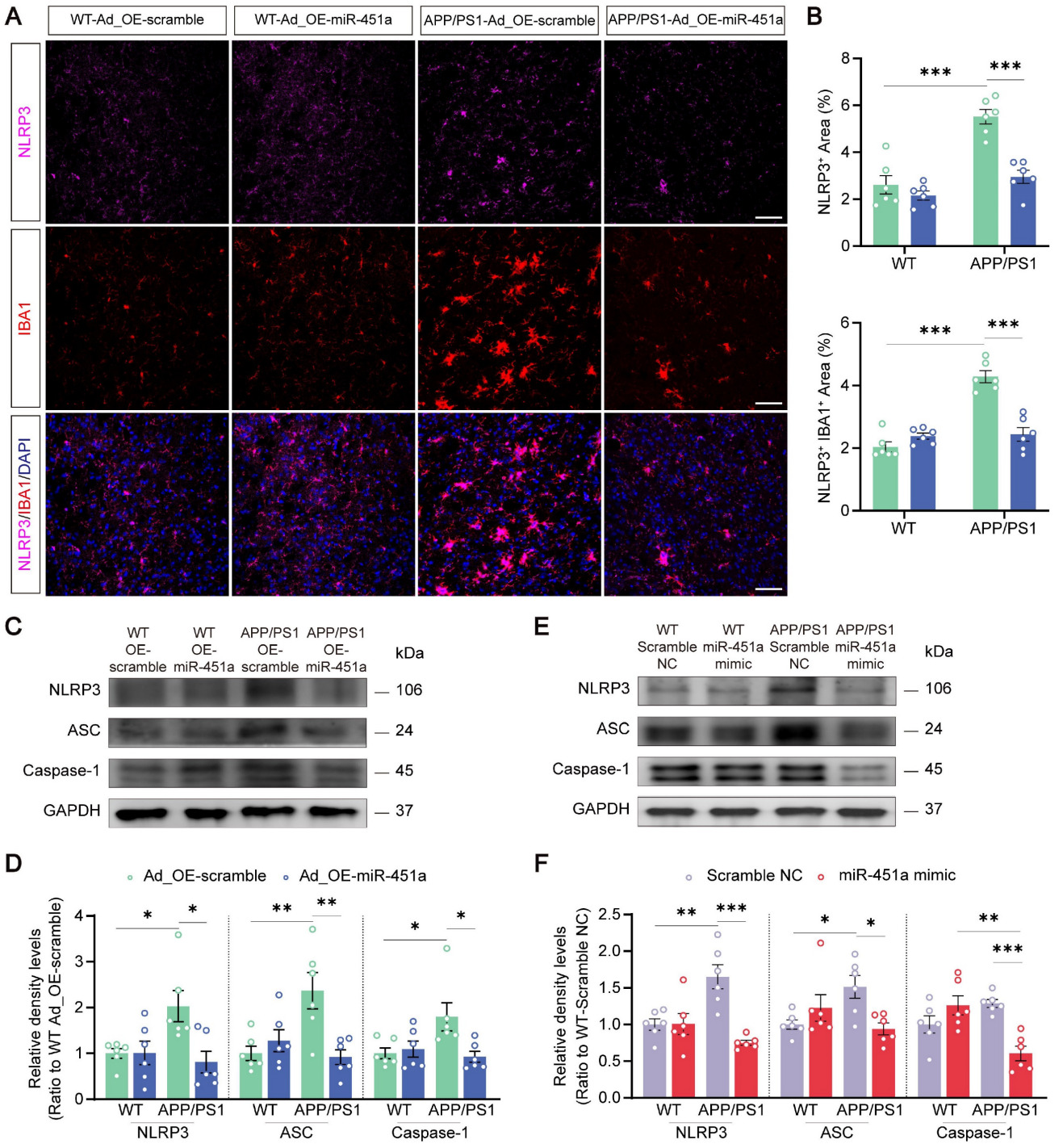

Figure 7. MiR-451a regulated neuroinflammation in the microglia via NLRP3/ASC/Caspase-1 pathway. (A) Representative image of NLRP3 (Magenta), IBA1 (Red), and DAPI (Blue) in the mPFC of each group. Scale bar, 50 μm. **(B)** The percentage of NLRP3$^+$ and NLRP3$^+$IBA1$^+$ area in the mPFC. **(C, D)** Representative Western blot bands and densitometry analysis of NLRP3, ASC, and Caspase-1 in the mPFC of each group. **(E, F)** Representative Western blot bands and densitometry analysis of NLRP3, ASC, and Caspase-1 in the primary microglia after treatment of miR-451a mimic. Data are presented as mean ± SEM. n = 6 per group. Significance was evaluated with two-way ANOVA with Tukey post-hoc test. *p <0.05, **p < 0.01, ***p < 0.001.

MiR-451a is located on the long arm of chromosome 17 and is enriched in blood, the pancreas, and other tissues [62-64]. MiR-451a is also expressed in brain tissue. We found that miR-451a was specifically expressed in the neurons and microglia, consistent with the previous reports [50, 65]. Alterations of miR-451a are observed in systemic lupus erythematosus, rheumatoid arthritis, and other diseases [63, 66]. In 2008, Cogswell et al. first reported that miR-451 decreased in the CSF of AD patients [33], which was confirmed by subsequent studies [67]. In addition, the proportion of patients with EOAD in our study was high, reaching 60%. This is because the majority of elderly LOAD patients are reluctant to

receive CSF puncture surgery mainly due to poor overall physical health status. We further confirmed the decrease in miR-451a CSF levels in patients with EOAD and LOAD and found no significant difference between the two types of AD, which is consistent with previous literature [60].

Although a large amount of literature reported dysregulation of miR-451a in patients with AD, its contribution to AD-related pathology remained elusive. Therefore, in this study, we characterized dynamic changes of miR-451a in the blood and CSF of APP/PS1 mice, an extensively used AD mouse model. We further demonstrated that miR-451a was down-regulated in both mPFC neurons and microglia of APP/PS1 mice from the age of 7 months. Still, the underlying mechanism of its down-regulation needs further exploration.

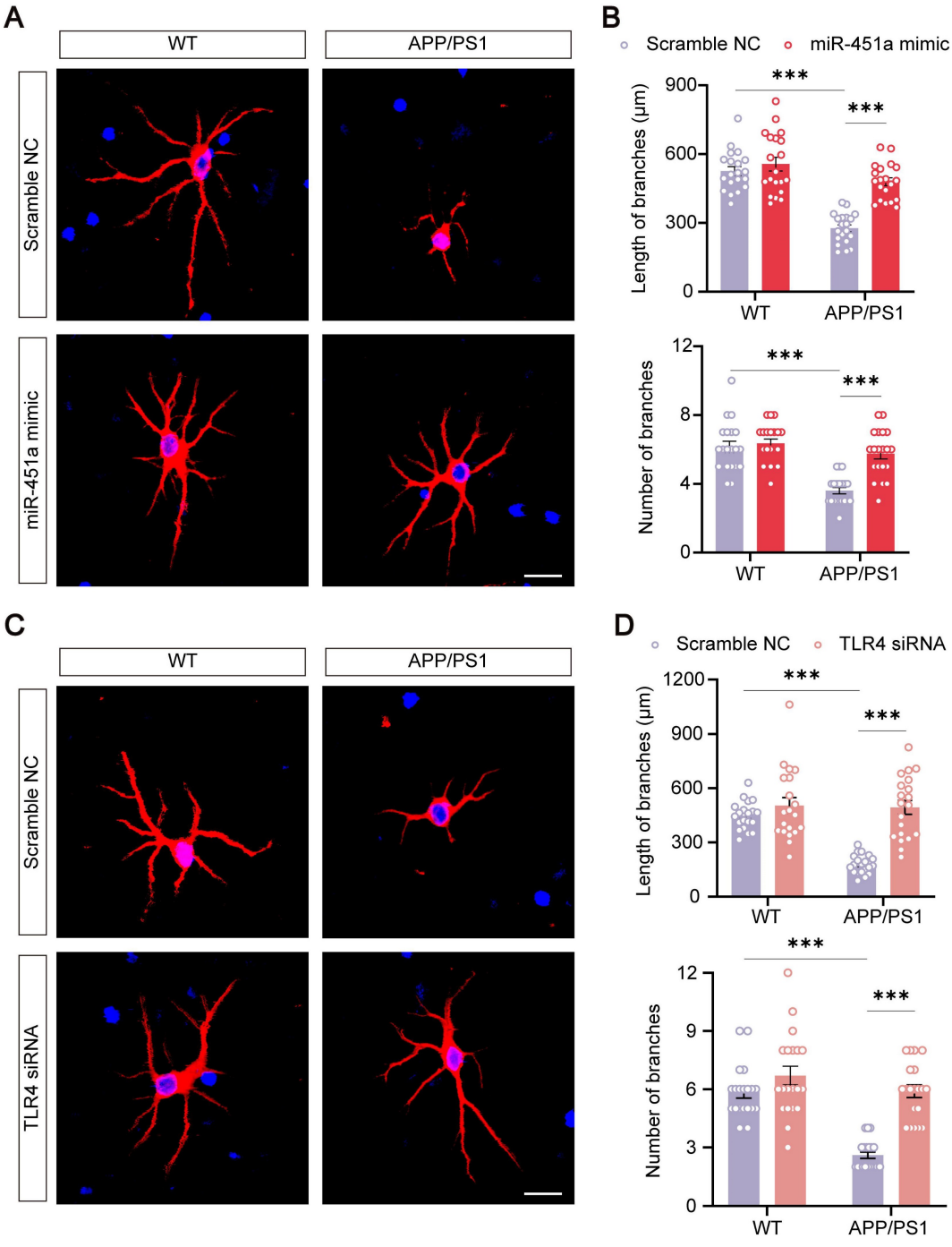

Figure 8. MiR-451a protected against neuritic atrophy in primary neurons of APP/PS1 mice. (A) Representative images of MAP2 of primary neurons treated with either miR-451a mimic (50 nM) or scramble NC. Scale bar, 20 μm. **(B)** Quantification of the neuritic length and branches number of primary neurons after miR-451a mimic treatment. **(C)** Representative images of MAP2 of primary neurons treated with either TLR4 siRNA (100 nM) or scramble NC. Scale bar, 20 μm. **(D)** Quantification of the neuritic length and branches number of primary neurons after TLR4 siRNA treatment. Data are presented as mean ± SEM. n = 20 per group. Significance was evaluated with two-way ANOVA with Tukey post-hoc test. ***$p < 0.001$.

Recent studies have shown that RNA degradation is enhanced in the brain of AD patients [68]. The stability of miRNAs in the brain depends largely on the two RNA-binding proteins, RBFOX and ZFP36. The imbalance of RBFOX1 has been shown to cause the instability of the miRNAs that regulate the gene expression of synaptic plasticity-related proteins, subsequently impairing synaptic function in AD [68]. In addition, miR-451a is negatively regulated by DNMT3B in bladder cancer [69]. DNMT3B, as a DNA methylation enzyme, increases the risk of AD by interacting with the APOE4 [70] and is up-regulated in peripheral blood mononuclear cells in LOAD patients [71]. Therefore, it is worth further studying whether RBFOX1 and/or DNMT3B affect brain miR-451a expression during AD.

Previous literature reported that 7-month-old APP/PS1 mice showed a significant increase in BACE1 expression in the mPFC [72], which is consistent with the current finding. Increased BACE1 expression promotes Aβ production, and secondary neuroinflammation, synapse and dendritic degeneration [72, 73]. It has been reported that miR-451a is down regulated in glioma, and overexpression of miR-451a can target IKKβ via NF-κB signal pathway, thereby inhibiting the growth of glioma cells *in vitro* and *in vivo* [74]. We found that miR-451a inhibited IKKβ/NF-κB signal pathway via decreasing TLR4 expression, subsequently down-regulating BACE1 and reducing Aβ production. In addition, high BACE1 level is also detected in the peripheral blood of patients with depression [75]. It remains to be determined whether alterations of BACE1 expression are involved in the depression-like phenotype of AD mice.

In addition to neurons, previous literature suggested that miR-451a regulates the activation of microglia in animal models of chronic pain [49], spinal cord injury [50], and gliomas [76]. Our results indicated that overexpression of miR-451a in APP/PS1 mice reduced the inflammatory response and NLRP3 activation. Overexpression of miRNA-451a also markedly reduced the level of NLRP3 in primary microglia. This suggests that NLRP3 is another target of miR-451a. This conclusion has been reconfirmed in a recent study that miR-451 directly targets NLRP3 and suppresses NLRP3-induced production of the inflammatory cytokines IL-1β and IL-18 in a mouse model of spinal cord injury [50].

It has been reported that the mPFC is involved in various behavioral activities. For example, our recent study reported that altered miR-124/Nr4a1 signal in the mPFC was involved in social behavioral defects of socially isolated mice [77]. The mPFC pyramid neurons regulate the spatial working memory [78], and the initiation of triggering receptor expressed on myeloid cell-2 (TREM2) transcription by activation of nuclear factor erythroid 2-related factor 2 (Nrf2) increases the microglial M2 phenotype in the mPFC, thus ameliorating depression-like behavior [79]. In the current study, we found that overexpression of miR-451a in the mPFC could improve long-term memory, social ability, and depression-like behavior in APP/PS1 mice. It is known that memory is initially stored in the hippocampus, but over time, memory will slowly consolidate in the cortex for permanent storage [80]. In agreement with this view, overexpression of miRNA-451a in the mPFC only improves long-term memory defects without affecting the hippocampus-related short-term memory.

In conclusion, we identified that miRNA-451a was closely related to cognitive impairment and depression in AD patients. We further verified that miR-451a was involved in regulating long-term memory and depression-like phenotype in AD model mice. We also demonstrated that overexpression of miRNA-451a in the mPFC inhibited the production of BACE1 via TLR4/IKKβ/NF-κB pathway and the glial inflammatory response by down-regulating NLRP3 activation, thereby reducing the neuronal degeneration. These results have revealed miRNA-451a as a novel target for the prevention and treatment of AD, especially for those with coexisting symptoms of depression.

Abbreviations

AAV: Adeno-associated virus serotype; AD: Alzheimer's disease; ADAM10: A disintegrin and metalloprotease 10; AID: Agranular insular cortex, dorsal part; AIV: Agranular insular cortex, ventral part; APOE4: Apolipoprotein E 4; APP: Amyloid β precursor protein; ATF2: Activating transcription factor 2; BACE1: β-site APP cleaving enzyme 1; Cg1: Cingulate cortex, area 1; CI: Caudal interstitial; CSF: Cerebrospinal fluid; CT: Threshold cycle; CTF-β: β-C-terminal fragment; DAPI: 4′, 6-diamidino-2-phenylindole; DEn: Dorsal endopiriform nucleus; DI: Dysgranular insular cortex; DNMT3B: DNA Methyltransferase 3 Beta; ELISA: Enzyme-linked immunosorbent assay; EOAD: Early-Onset AD; FISH: Fluorescence in situ hybridization; FLI1: Friend leukemia integration 1; GAPDH: Glyceraldehyde-3-phosphate dehydrogenase; HAMD: Hamilton Depression Scale; HEK293: Human embryonic kidney cells; IBA1: Ionized calcium binding adapter molecule 1; IDE: Insulin-degrading enzyme; IKKβ: Inhibitor of kappa B Kinase β; IL: Infralimbic cortex; IL-1β: Interleukin-1β; IL-6: Interleukin-6; LO: Lateral orbital cortex; LOAD: Larly-Onset AD; LRP1: Low-density lipoprotein receptor related protein 1; M1: Primary

motor cortex; M2: Secondary motor cortex; MAP2: Microtubule Associated Protein 2; miRNA: microRNA; MoCA: Montreal Cognitive Assessment; mPFC: Medial prefrontal cortex; MYC: Myelocytomatosis oncogene; NEP: Neutral endopeptidase; NFIB: Nuclear factor I/B; NF-κB: Nuclear factor kappa-B; NLRP3: NOD-like receptor protein 3; Nrf2: Nuclear factor erythroid 2-related factor 2; PPARGC1A: Peroxisome proliferative activated receptor gamma co-activator 1 alpha; PrL: Prelimbic cortex; PS1: Presenilin-1; PSD95: Postsynaptic density protein 95; qRT-PCR: Quantitative real-time PCR; RBFOX1: RNA Binding Fox-1 Homolog 1; S1: Primary somatosensory cortex; sAPPβ: Soluble amyloid precursor protein beta; SCI: Spinal cord injury; Six1: Sine oculis homeobox 1; SYP: Synaptophysin; Tbx19: T-box 19; TLR4: Toll like receptor 4; TNF-α: Tumor necrosis factor-α; TREM2: Triggering receptor expressed on myeloid cell-2; WWTR1: WW domain containing transcription regulator 1; YBX1: Y box protein 1; ZFP36: Zinc Finger Protein 36; Zic3: Zinc finger protein of the cerebellum 3

Supplementary Material

Supplementary figures and tables.
https://www.thno.org/v13p3021s1.pdf

Acknowledgments

The authors would like to acknowledge the valuable suggestions from Prof. Ming Lu at Nanjing Medical University.

Funding

This work was supported by the National Natural Science Foundation of China (Grant NO. 81871117).

Author contributions

M.X., P.H., and H.F. conceived and designed the experiments. P.H., Y.C., Q.C., H.S., and H.F. conducted biochemistry experiments and behavior tests. J.C., X.H., and H.F. performed the immunostaining and cell culture. J.S., Y.Z., M.Y., and H.F. collected human CSF. M.X., C.S., J.G., Y.Z., Q.L., C.M., and H.F. wrote and modified the manuscript. All the authors contributed to the review of the manuscript.

Competing Interests

The authors have declared that no competing interest exists.

References

1. Fratiglioni L, Qiu C. Prevention of common neurodegenerative disorders in the elderly. Exp Gerontol. 2009; 44: 46-50.
2. Donovan NJ, Wadsworth LP, Lorius N, Locascio JJ, Rentz DM, Johnson KA, et al. Regional cortical thinning predicts worsening apathy and hallucinations across the Alzheimer disease spectrum. Am J Geriatr Psychiatry. 2014; 22: 1168-79.
3. Burhanullah MH, Tschanz JT, Peters ME, Leoutsakos JM, Matyi J, Lyketsos CG, et al. Neuropsychiatric symptoms as risk factors for cognitive decline in clinically normal older adults: The Cache County Study. Am J Geriatr Psychiatry. 2020; 28: 64-71.
4. Ismail Z, Smith EE, Geda Y, Sultzer D, Brodaty H, Smith G, et al. Neuropsychiatric symptoms as early manifestations of emergent dementia: Provisional diagnostic criteria for mild behavioral impairment. Alzheimers Dement. 2016; 12: 195-202.
5. Ismail Z, Gatchel J, Bateman DR, Barcelos-Ferreira R, Cantillon M, Jaeger J, et al. Affective and emotional dysregulation as pre-dementia risk markers: exploring the mild behavioral impairment symptoms of depression, anxiety, irritability, and euphoria. Int Psychogeriatr. 2018; 30: 185-96.
6. Jang JY, Ho JK, Blanken AE, Dutt S, Nation DA. Affective neuropsychiatric symptoms as early signs of dementia risk in older adults. J Alzheimers Dis. 2020; 77: 1195-207.
7. Naik S, Fuchs E. Inflammatory memory and tissue adaptation in sickness and in health. Nature. 2022; 607: 249-55.
8. Winter J, Jung S, Keller S, Gregory RI, Diederichs S. Many roads to maturity: microRNA biogenesis pathways and their regulation. Nat Cell Biol. 2009; 11: 228-34.
9. Zheng K, Hu F, Zhou Y, Zhang J, Zheng J, Lai C, et al. MiR-135a-5p mediates memory and synaptic impairments via the Rock2/Adducin1 signaling pathway in a mouse model of Alzheimer's disease. Nat Commun. 2021; 12: 1903.
10. Fan C, Li Y, Lan T, Wang W, Long Y, Yu SY. Microglia secrete miR-146a-5p-containing exosomes to regulate neurogenesis in depression. Mol Ther. 2022; 30: 1300-14.
11. Cha DJ, Mengel D, Mustapic M, Liu W, Selkoe DJ, Kapogiannis D, et al. MiR-212 and miR-132 are downregulated in neurally derived plasma exosomes of Alzheimer's patients. Front Neurosci. 2019; 13: 1208.
12. Derkow K, Rössling R, Schipke C, Krüger C, Bauer J, Fähling M, et al. Distinct expression of the neurotoxic microRNA family let-7 in the cerebrospinal fluid of patients with Alzheimer's disease. PLoS One. 2018; 13: e0200602.
13. Wang X, Liu D, Huang HZ, Wang ZH, Hou TY, Yang X, et al. A novel microRNA-124/PTPN1 signal pathway mediates synaptic and memory deficits in Alzheimer's disease. Biol Psychiatry. 2018; 83: 395-405.
14. He L, Chen Z, Wang J, Feng H. Expression relationship and significance of NEAT1 and miR-27a-3p in serum and cerebrospinal fluid of patients with Alzheimer's disease. BMC Neurol. 2022; 22: 203.
15. He S, Liu X, Jiang K, Peng D, Hong W, Fang Y, et al. Alterations of microRNA-124 expression in peripheral blood mononuclear cells in pre- and post-treatment patients with major depressive disorder. J Psychiatr Res. 2016; 78: 65-71.
16. Ding Y, Zhong M, Qiu B, Liu C, Wang J, Liang J. Abnormal expression of miR-135a in patients with depression and its possible involvement in the pathogenesis of the condition. Exp Ther Med. 2021; 22: 726.
17. Liang Y, Zhao G, Sun R, Mao Y, Li G, Chen X, et al. Genetic variants in the promoters of let-7 family are associated with an increased risk of major depressive disorder. J Affect Disord. 2015; 183: 295-9.
18. Fang Y, Qiu Q, Zhang S, Sun L, Li G, Xiao S, et al. Changes in miRNA-132 and miR-124 levels in non-treated and citalopram-treated patients with depression. J Affect Disord. 2018; 227: 745-51.
19. Li Y, Song W, Tong Y, Zhang X, Zhao J, Gao X, et al. Isoliquiritin ameliorates depression by suppressing NLRP3-mediated pyroptosis via miRNA-27a/SYK/NF-κB axis. J Neuroinflammation. 2021; 18: 1.
20. Jack CR, Jr., Bennett DA, Blennow K, Carrillo MC, Dunn B, Haeberlein SB, et al. NIA-AA research framework: Toward a biological definition of Alzheimer's disease. Alzheimers Dement. 2018; 14: 535-62.
21. Fasnacht JS, Wueest AS, Berres M, Thomann AE, Krumm S, Gutbrod K, et al. Conversion between the Montreal Cognitive Assessment and the Mini-Mental Status Examination. J Am Geriatr Soc. 2023; 71: 869-79.
22. Lin J, Wang X, Dong F, Du Y, Shen J, Ding S, et al. Validation of the Chinese version of the Hamilton Rating Scale for depression in adults with epilepsy. Epilepsy Behav. 2018; 89: 148-52.
23. Liu WZ, Zhang WH, Zheng ZH, Zou JX, Liu XX, Huang SH, et al. Identification of a prefrontal cortex-to-amygdala pathway for chronic stress-induced anxiety. Nat Commun. 2020; 11: 2221.
24. Moser PC. An evaluation of the elevated plus-maze test using the novel anxiolytic buspirone. Psychopharmacology (Berl). 1989; 99: 48-53.
25. Leger M, Quiedeville A, Bouet V, Haelewyn B, Boulouard M, Schumann-Bard P, et al. Object recognition test in mice. Nat Protoc. 2013; 8: 2531-7.
26. Sarnyai Z, Sibille EL, Pavlides C, Fenster RJ, McEwen BS, Toth M. Impaired hippocampal-dependent learning and functional abnormalities in the hippocampus in mice lacking serotonin(1A) receptors. Proc Natl Acad Sci U S A. 2000; 97: 14731-6.
27. Leung C, Kim JC, Jia Z. Three-chamber social approach task with optogenetic stimulation (mice). Bio Protoc. 2018; 8: e3120.
28. Liu MY, Yin CY, Zhu LJ, Zhu XH, Xu C, Luo CX, et al. Sucrose preference test for measurement of stress-induced anhedonia in mice. Nat Protoc. 2018; 13: 1686-98.

29. Petit-Demouliere B, Chenu F, Bourin M. Forced swimming test in mice: a review of antidepressant activity. Psychopharmacology (Berl). 2005; 177: 245-55.
30. Liu D, Tang H, Li XY, Deng MF, Wei N, Wang X, et al. Targeting the HDAC2/HNF-4A/miR-101b/AMPK pathway rescues tauopathy and dendritic abnormalities in Alzheimer's disease. Mol Ther. 2017; 25: 752-64.
31. Volpicelli-Daley LA, Luk KC, Lee VM. Addition of exogenous α-synuclein preformed fibrils to primary neuronal cultures to seed recruitment of endogenous α-synuclein to Lewy body and Lewy neurite-like aggregates. Nat Protoc. 2014; 9: 2135-46.
32. Han X, Xu T, Ding C, Wang D, Yao G, Chen H, et al. Neuronal NR4A1 deficiency drives complement-coordinated synaptic stripping by microglia in a mouse model of lupus. Signal Transduct Target Ther. 2022; 7: 50.
33. Cogswell JP, Ward J, Taylor IA, Waters M, Shi Y, Cannon B, et al. Identification of miRNA changes in Alzheimer's disease brain and CSF yields putative biomarkers and insights into disease pathways. J Alzheimers Dis. 2008; 14: 27-41.
34. Wan Y, Liu Y, Wang X, Wu J, Liu K, Zhou J, et al. Identification of differential microRNAs in cerebrospinal fluid and serum of patients with major depressive disorder. PLoS One. 2015; 10: e0121975.
35. Belzeaux R, Bergon A, Jeanjean V, Loriod B, Formisano-Tréziny C, Verrier L, et al. Responder and nonresponder patients exhibit different peripheral transcriptional signatures during major depressive episode. Transl Psychiatry. 2012; 2: e185.
36. Nan Y, Guo L, Lu Y, Guo G, Hong R, Zhao L, et al. MiR-451 suppresses EMT and metastasis in glioma cells. Cell Cycle. 2021; 20: 1270-8.
37. Wang X, Hong Y, Wu L, Duan X, Hu Y, Sun Y, et al. Deletion of microRNA-144/451 cluster aggravated brain injury in intracerebral hemorrhage mice by targeting 14-3-3ζ. Front Neurol. 2020; 11: 551411.
38. Fu C, Chen S, Cai N, Liu Z, Wang P, Zhao J. Potential neuroprotective effect of miR-451 against cerebral ischemia/reperfusion injury in stroke patients and a mouse model. World Neurosurg. 2019; 130: e54-e61.
39. Pini L, Pievani M, Bocchetta M, Altomare D, Bosco P, Cavedo E, et al. Brain atrophy in Alzheimer's disease and aging. Ageing Res Rev. 2016; 30: 25-48.
40. Palazidou E. The neurobiology of depression. Br Med Bull. 2012; 101: 127-45.
41. Sapolsky RM. Depression, antidepressants, and the shrinking hippocampus. Proc Natl Acad Sci U S A. 2001; 98: 12320-2.
42. Pugh PL, Richardson JC, Bate ST, Upton N, Sunter D. Non-cognitive behaviours in an APP/PS1 transgenic model of Alzheimer's disease. Behav Brain Res. 2007; 178: 18-28.
43. Gao JY, Chen Y, Su DY, Marshall C, Xiao M. Depressive- and anxiety-like phenotypes in young adult APP(Swe)/PS1(dE9) transgenic mice with insensitivity to chronic mild stress. Behav Brain Res. 2018; 353: 114-23.
44. Slack FJ, Chinnaiyan AM. The role of non-coding RNAs in oncology. Cell. 2019; 179: 1033-55.
45. Chen CH, Zhou W, Liu S, Deng Y, Cai F, Tone M, et al. Increased NF-κB signalling up-regulates BACE1 expression and its therapeutic potential in Alzheimer's disease. Int J Neuropsychopharmacol. 2012; 15: 77-90.
46. Rehman MU, Sehar N, Dar NJ, Khan A, Arafah A, Rashid S, et al. Mitochondrial dysfunctions, oxidative stress and neuroinflammation as therapeutic targets for neurodegenerative diseases: An update on current advances and impediments. Neurosci Biobehav Rev. 2022; 144: 104961.
47. Kaufmann FN, Costa AP, Ghisleni G, Diaz AP, Rodrigues ALS, Peluffo H, et al. NLRP3 inflammasome-driven pathways in depression: Clinical and preclinical findings. Brain Behav Immun. 2017; 64: 367-83.
48. Thounaojam MC, Kaushik DK, Basu A. MicroRNAs in the brain: It's regulatory role in neuroinflammation. Mol Neurobiol. 2013; 47: 1034-44.
49. Sun X, Zhang H. MiR-451 elevation relieves inflammatory pain by suppressing microglial activation-evoked inflammatory response via targeting TLR4. Cell Tissue Res. 2018; 374: 487-95.
50. Hong Z, Cheng J, Ye Y, Chen X, Zhang F. MicroRNA-451 attenuates the inflammatory response of activated microglia by downregulating nucleotide binding oligomerization domain-like receptor protein 3. World Neurosurg. 2022; 167: e1128-e37.
51. Misrani A, Tabassum S, Huo Q, Tabassum S, Jiang J, Ahmed A, et al. Mitochondrial deficits with neural and social damage in early-stage Alzheimer's disease model mice. Front Aging Neurosci. 2021; 13: 748388.
52. Kommaddi RP, Tomar DS, Karunakaran S, Bapat D, Nanguneri S, Ray A, et al. Glutaredoxin1 diminishes amyloid beta-mediated oxidation of F-actin and reverses cognitive deficits in an Alzheimer's disease mouse model. Antioxid Redox Signal. 2019; 31: 1321-38.
53. Ding S, Yang L, Huang L, Kong L, Chen M, Su Y, et al. Chronic glucocorticoid exposure accelerates Aβ generation and neurotoxicity by activating calcium-mediated CN-NFAT1 signaling in hippocampal neurons in APP/PS1 mice. Food Chem Toxicol. 2022; 168: 113407.
54. Kashyap G, Bapat D, Das D, Gowaikar R, Amritkar RE, Rangarajan G, et al. Synapse loss and progress of Alzheimer's disease -A network model. Sci Rep. 2019; 9: 6555.
55. Chi S, Yu JT, Tan MS, Tan L. Depression in Alzheimer's disease: Epidemiology, mechanisms, and management. J Alzheimers Dis. 2014; 42: 739-55.
56. Van der Mussele S, Bekelaar K, Le Bastard N, Vermeiren Y, Saerens J, Somers N, et al. Prevalence and associated behavioral symptoms of depression in mild cognitive impairment and dementia due to Alzheimer's disease. Int J Geriatr Psychiatry. 2013; 28: 947-58.
57. Chen ML, Hong CG, Yue T, Li HM, Duan R, Hu WB, et al. Inhibition of miR-331-3p and miR-9-5p ameliorates Alzheimer's disease by enhancing autophagy. Theranostics. 2021; 11: 2395-409.
58. Walgrave H, Balusu S, Snoeck S, Vanden Eynden E, Craessaerts K, Thrupp N, et al. Restoring miR-132 expression rescues adult hippocampal neurogenesis and memory deficits in Alzheimer's disease. Cell Stem Cell. 2021; 28: 1805-21.e8.
59. Sun T, Zhao K, Liu M, Cai Z, Zeng L, Zhang J, et al. MiR-30a-5p induces Aβ production via inhibiting the nonamyloidogenic pathway in Alzheimer's disease. Pharmacol Res. 2022; 178: 106153.
60. McKeever PM, Schneider R, Taghdiri F, Weichert A, Multani N, Brown RA, et al. MicroRNA expression levels are altered in the cerebrospinal fluid of patients with young-onset Alzheimer's disease. Mol Neurobiol. 2018; 55: 8826-41.
61. Wang L, Zhen H, Sun Y, Rong S, Li B, Song Z, et al. Plasma exo-miRNAs correlated with AD-related factors of Chinese individuals involved in Aβ accumulation and cognition decline. Mol Neurobiol. 2022; 59: 6790-804.
62. Chakraborty S, Basu A. MiR-451a regulates neuronal apoptosis by modulating 14-3-3ζ-JNK axis upon flaviviral infection. mSphere. 2022; 7: e0020822.
63. Prajzlerová K, Kryštůfková O, Hánová P, Horváthová V, Gregová M, Pavelka K, et al. High miR-451 expression in peripheral blood mononuclear cells from subjects at risk of developing rheumatoid arthritis. Sci Rep. 2021; 11: 4719.
64. Ali S, Saleh H, Sethi S, Sarkar FH, Philip PA. MicroRNA profiling of diagnostic needle aspirates from patients with pancreatic cancer. Br J Cancer. 2012; 107: 1354-60.
65. Liu Q, Hu Y, Zhang M, Yan Y, Yu H, Ge L. MicroRNA-451 protects neurons against ischemia/reperfusion injury-induced cell death by targeting CELF2. Neuropsychiatr Dis Treat. 2018; 14: 2773-82.
66. Tan L, Zhao M, Wu H, Zhang Y, Tong X, Gao L, et al. Downregulated serum exosomal miR-451a expression correlates with renal damage and its intercellular communication role in systemic lupus erythematosus. Front Immunol. 2021; 12: 630112.
67. Gámez-Valero A, Campdelacreu J, Vilas D, Ispierto L, Reñé R, Álvarez R, et al. Exploratory study on microRNA profiles from plasma-derived extracellular vesicles in Alzheimer's disease and dementia with Lewy bodies. Transl Neurodegener. 2019; 8: 31.
68. Alkallas R, Fish L, Goodarzi H, Najafabadi HS. Inference of RNA decay rate from transcriptional profiling highlights the regulatory programs of Alzheimer's disease. Nat Commun. 2017; 8: 909.
69. Liu B, Sun W, Gao W, Li L, Cao Z, Yang X, et al. MicroRNA-451a promoter methylation regulated by DNMT3B expedites bladder cancer development via the EPHA2/PI3K/AKT axis. BMC Cancer. 2020; 20: 1019.
70. de Bem CM, Pezzi JC, Borba EM, Chaves ML, de Andrade FM, Fiegenbaum M, et al. The synergistic risk effect of apolipoprotein ε4 and DNA (cytosine-5-)-methyltransferase 3 beta (DNMT3B) haplotype for Alzheimer's disease. Mol Biol Rep. 2016; 43: 653-8.
71. Di Francesco A, Arosio B, Falconi A, Micioni Di Bonaventura MV, Karimi M, Mari D, et al. Global changes in DNA methylation in Alzheimer's disease peripheral blood mononuclear cells. Brain Behav Immun. 2015; 45: 139-44.
72. Mahaman YAR, Feng J, Huang F, Salissou MTM, Wang J, Liu R, et al. Moringa oleifera alleviates Aβ burden and improves synaptic plasticity and cognitive impairments in APP/PS1 mice. Nutrients. 2022; 14: 20.
73. Blume T, Filser S, Jaworska A, Blain JF, Koenig G, Moschke K, et al. BACE1 inhibitor MK-8931 alters formation but not stability of dendritic spines. Front Aging Neurosci. 2018; 10: 229.
74. Nan Y, Guo L, Zhen Y, Wang L, Ren B, Chen X, et al. MiRNA-451 regulates the NF-κB signaling pathway by targeting IKKβ to inhibit glioma cell growth. Cell Cycle. 2021; 20: 1967-77.
75. Ghafouri-Fard S, Taheri M, Arsang-Jang S, Kholghi Oskooei V, Omrani MD. Sex-based dimorphisms in expression of BDNF and BACE1 in bipolar patients. Compr Psychiatry. 2019; 91: 29-33.
76. Buruiană A, Florian Ş I, Florian AI, Timiş TL, Mihu CM, Micläuş M, et al. The roles of miRNA in glioblastoma tumor cell communication: diplomatic and aggressive negotiations. Int J Mol Sci. 2020; 21: 6.
77. Zhang Y, Pang Y, Feng W, Jin Y, Chen S, Ding S, et al. MiR-124 regulates early isolation-induced social abnormalities via inhibiting myelinogenesis in the medial prefrontal cortex. Cell Mol Life Sci. 2022; 79: 507.
78. Vogel P, Hahn J, Duvarci S, Sigurdsson T. Prefrontal pyramidal neurons are critical for all phases of working memory. Cell Rep. 2022; 39: 110659.
79. He L, Zheng Y, Huang L, Ye J, Ye Y, Luo H, et al. Nrf2 regulates the arginase 1^{+} microglia phenotype through the initiation of TREM2 transcription, ameliorating depression-like behavior in mice. Transl Psychiatry. 2022; 12: 459.
80. Kitamura T, Ogawa SK, Roy DS, Okuyama T, Morrissey MD, Smith LM, et al. Engrams and circuits crucial for systems consolidation of a memory. Science. 2017; 356: 73-8.
81. Lv Z, Hu L, Yang Y, Zhang K, Sun Z, Zhang J, et al. Comparative study of microRNA profiling in one Chinese family with PSEN1 G378E mutation. Metab Brain Dis. 2018; 33: 1711-20.
82. Hu J, Zhou Z, Yang Q, Yang K. Differential expression of miR-30a-5p in post stroke depression and bioinformatics analysis of the possible mechanism. Nan Fang Yi Ke Da Xue Xue Bao. 2020; 40: 922-9.
83. Maffioletti E, Cattaneo A, Rosso G, Maina G, Maj C, Gennarelli M, et al. Peripheral whole blood microRNA alterations in major depression and bipolar disorder. J Affect Disord. 2016; 200: 250-8.

84. Kmetzsch V, Anquetil V, Saracino D, Rinaldi D, Camuzat A, Gareau T, et al. Plasma microRNA signature in presymptomatic and symptomatic subjects with C9orf72-associated frontotemporal dementia and amyotrophic lateral sclerosis. J Neurol Neurosurg Psychiatry. 2021; 92: 485-93.
85. Denk J, Boelmans K, Siegismund C, Lassner D, Arlt S, Jahn H. MicroRNA profiling of CSF reveals potential biomarkers to detect Alzheimer's disease. PLoS One. 2015; 10: e0126423.
86. Ebrahimkhani S, Vafaee F, Young PE, Hur SSJ, Hawke S, Devenney E, et al. Exosomal microRNA signatures in multiple sclerosis reflect disease status. Sci Rep. 2017; 7: 14293.
87. Prabhakar P, Chandra SR, Christopher R. Circulating microRNAs as potential biomarkers for the identification of vascular dementia due to cerebral small vessel disease. Age Ageing. 2017; 46: 861-4.
88. Liguori M, Nuzziello N, Introna A, Consiglio A, Licciulli F, D'Errico E, et al. Dysregulation of microRNAs and target genes networks in peripheral blood of patients with sporadic amyotrophic lateral sclerosis. Front Mol Neurosci. 2018; 11: 288.
89. Saeedi S, Nagy C, Ibrahim P, Théroux JF, Wakid M, Fiori LM, et al. Neuron-derived extracellular vesicles enriched from plasma show altered size and miRNA cargo as a function of antidepressant drug response. Mol Psychiatry. 2021; 26: 7417-24.
90. Peña-Bautista C, Tarazona-Sánchez A, Braza-Boils A, Balaguer A, Ferré-González L, Cañada-Martínez AJ, et al. Plasma microRNAs as potential biomarkers in early Alzheimer disease expression. Sci Rep. 2022; 12: 15589.